

Chapter 4

Enantio-selective laser control mechanisms for the model system H_2POSH

4.1 Outline of the chapter

The investigations on laser control for the selective preparation of enantiomers starts with the choice of an appropriate model system. This chapter introduces the reader to the first molecular model system H_2POSH (section 4.2) for which two fundamental laser control schemes for the purification of a racemate were developed, namely, the so-called “parking” mechanism (section 4.6) and the enantio-selective pump-dump mechanism (section 4.7). Before the laser driven dynamics are considered (section 4.5) the potential energy curves along the reaction path have to be obtained (section 4.3) and the time-independent Schrödinger equation for the model has to be solved (section 4.4). The chapter finishes with considerations for an experimental setup to proof the success of the theoretically obtained laser control schemes (section 4.8).

4.2 Choice of a model system

The choice of a molecular model system for the purpose of this work must be based on certain criteria (a-c). (a) The molecule needs to be chiral, but there should be only one molecular source of chirality within the molecule. More than one chiral center results in more than two stereo-isomers (two or more diastereomeric pairs of enantiomers) making the model unnecessarily complicated. There are different types of chiral elements that may be used for a model system. The choice influences the reaction path transforming the enantiomer from one configuration to the other. In order to transform a chiral center, e.g. a carbon atom with four different substituents, from its *R*-form into its *S*-form or *vice versa*, at least one chemical bond has to be broken and reconnected on “the other side” of the molecule. The description of such a reaction path is rather complicated since it includes dissociation as well as bond formation plus the movement of two fragments relative to each other. Therefore, criterion (b) is the desire to develop a chiral model system in such a way that the reaction path transforming both enantiomers into each other is easy to be described by means of quantum dynamics. A chiral axis allows to simplify the reaction path to a relative torsional motion of two fragments of the molecule around the chiral axis. Molecules with chiral axis form only stable enantiomers (called atropisomers¹), i.e. the time for the transformation from one stereo-isomer to the other is longer than the time for the observation or reaction, if the torsional barrier for the chiral axis is high enough. This torsional barrier depends on the molecular fragments the molecule consists of. Substituents with large steric expansion may hinder the torsional motion at room temperature. Such substituents usually consist of many atoms or of atoms with high atomic number. However, criterion (c) is to keep the molecular model system “small” enough to be described by the means of quantum mechanics. The more electrons are included in the quantum chemistry calculations the larger is the computational effort. Therefore, the model system should not consist of more atoms than needed to investigate the problem and if possible of light atoms.

There are more criteria (d-f) which are more difficult to fulfill but they intend to make the model more realistic in terms of an experiment: (d) As discussed in section 3.4 the lifetime of an enantiomer depends on the tunneling time of its corresponding localized wave function tunneling between both minima of the double well potential. The potential barrier between both minima controls this tunneling time and hence, the lifetime of the enantiomers; the higher this barrier is, the longer the lifetime. To monitor the successful preparation of a pure enantiomer by means of spectroscopy the lifetime of the enantiomer should be sufficiently long (at least 100 ps). Therefore, the potential barrier must be

¹Isomers that can be separated only because rotation about a single bond is prevented or greatly slowed are called atropisomers (for a review see ref. [124])

high enough to support a localized wave packet that does not tunnel so fast that the enantiomer described by this wave packet cannot be observed by experimental methods. (e) In order to have sufficient control over the molecular system a strong coupling of the its dipole moment with the laser field is necessary, especially along the reaction path. Weak couplings with the laser field lead to high laser intensities that may lead to ionization or dissociation of the molecule. Therefore, the dipole moments should undergo a sufficiently large change (± 1 Debye or more) along the path from one enantiomer to the other. (f) Finally, the model system should have similarities with experimentally commonly used ones or, at least, with molecules which are experimentally easily available. Only then the results from theoretical calculations may motivate experimentalists to carry out experiments based on these results.

In this chapter the first model system to describe the purification of a racemate by laser pulses will be discussed. It is a rather simple model, yet convenient for developing laser control mechanisms. Unfortunately, it gives little possibilities for experimental investigation. In the following chapter 5 a more complicated model will be presented, which allows more connections between theory and experiment.

The model system chosen first is the thiophosphinic acid H_2POSH . This molecule is chiral because it has a chiral axis along its P-S bond. Below room temperature it forms two stable conformers (atropisomers) as shown in figure 4.1. Each of them is the mirror image of the other, still they are not identical molecules. The two conformations shown in figure 4.1 are the minimum energy configuration of both enantiomers. A torsional motion of the H around the P-S bond, keeping the H_2PO -group fixed, converts one enantiomer into the other.

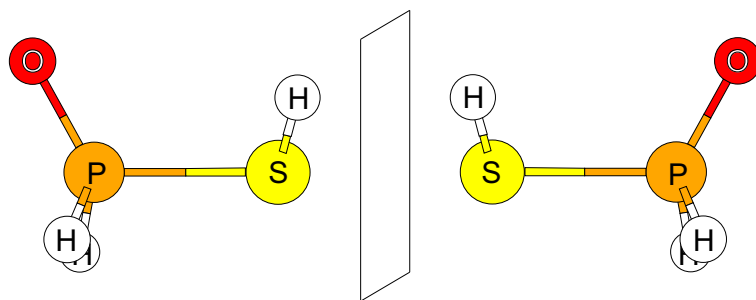


Figure 4.1: Enantiomers of the H_2POSH molecule

This model system fulfills criteria a-c: (a) It is chiral with one single chiral element, namely a chiral axis. This allows a simple reaction path (b): a one-dimensional motion (the torsion of the terminal Hydrogen relative to the rest) describes the conversion be-

tween both enantiomers. Since the molecule only consists of six atoms with an overall of 42 electrons, it is possible to calculate its potential energy surfaces with a bearable computational effort, in accordance with criterion (c).

Since criteria (d) and (e) depend on the barrier height of the potential energy curve and on the dipole moments, respectively, they will be discussed in more detail in the following section. Here, suffice it to say that both criteria are fulfilled; (d) because the potential barrier is about 500 cm⁻¹ allowing sufficiently long tunneling times, at least for the lowest doublet of eigenstates; and (e) because the change of at least two dipole moment components along the reaction path are sufficiently large to allow strong coupling with the laser field.

For the case of H₂POSH criterion (f) is only partly fulfilled. Thiophosphinic acid can be synthesized in the laboratory, still it is a rather difficult substance to handle because it is very reactive. It cannot be handled in an air environment because it will instantaneously react with oxygen eventually forming SO₂ and H₃PO₄. The preparation of a pure enantiomer of H₂POSH by experimental means seems to be impossible since there is no known way to synthesize it via a stereo-specific reaction or to isolate it from a racemic mixture. At room temperature H₂POSH is not chiral because the states above the potential barrier are also populated making the molecule on a time average achiral. Therefore, the chosen model system is not the best choice for an experiment; it covers in most but not in all parts the behavior of “realistic” chiral molecules. This problem is overcome in chapter 5 where a more “realistic” model system will be presented.

4.3 Potential energy curves for S₀ and S₁

In all calculations the model system H₂POSH is assumed to be oriented with its P-S bond along the z-axis while the OPS fragment lies in the xz-plane as shown in figure 4.2. The dihedral angle OPSH, called ϕ , is used to describe the torsional motion of the terminal hydrogen around the P-S bond. The angle ϕ is defined such that it is zero if the fragment OPSH is in the xz-plane with the terminal hydrogen pointing in positive x-direction. This is called the *cis*-conformation of the molecule in analogy to the nomenclature of *cis*-*trans* stereo-isomers. If the terminal hydrogen is pointing in negative x-direction still being in the xz-plane, it is called the *trans*-conformation, with the angle ϕ being either -180° or $+180^\circ$ depending on the direction of torsion starting from the *cis*-conformation. The *cis*- and *trans*-conformations of H₂POSH, calculated by MP2 at the 6-311G(2d,p) level of theory, are shown in figure 4.3. At $\phi = 0^\circ$ and $\pm 180^\circ$, respectively, the molecule has C_S-symmetry with the OPSH fragment in the mirror plane. Hence, these conformations

are *achiral*. The two stable chiral forms of the molecule are at $\phi = -59.5^\circ$ corresponding to the *L*-enantiomer and at $\phi = +59.5^\circ$ corresponding to the *R*-enantiomer. Their relaxed geometries, depicted in figure 4.4, are optimized by MP2 using the 6-311G(2d,p) basis set. In order to obtain a *symmetric* double well potential curve along ϕ from *ab initio* calculations a *symmetric* geometry (with respect to the *xz*-plane) for the *non-moving* parts of the molecule is required as reference. This *symmetric* geometry is derived by taking the arithmetic average of the P-H bond distances as well as of the HPS-angles of both relaxed geometries in fig. 4.4.

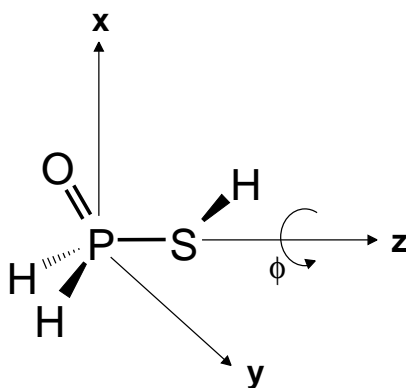


Figure 4.2: Model system H_2POSH fixed in the *x,y,z*-coordinate system

The unrelaxed potential energy curves along the angle ϕ for the electronic ground state S_0 and the first electronic excited singlet state S_1 are calculated by means of (TD-)DFT (see section 2.2.7) using the *symmetric* geometry of the *L*-enantiomer of the electronic ground state as a reference [125].² Except for the torsional dihedral angle ϕ all geometrical parameters are frozen, with the P-H bond length and HPS angle fixed to the values of the *symmetric* geometry. Both singlet states were calculated at the B3LYP/6-311+G(2d,p) level of theory. The resulting energy curves $V_0(\phi)$ and $V_1(\phi)$ are shown in Figure 4.5. The Newman projection of the two enantiomers correspond to the minima at -65° and $+65^\circ$ of the electronic ground state. The central potential barrier of V_0 at $\phi = 0^\circ$ has a height of 519.4 cm^{-1} , while the other barrier at $\phi = \pm 180^\circ$ is 984.1 cm^{-1} high. The electronic excited potential energy curve $V_1(\phi)$ has a single minimum where $V_0(\phi)$ has its lower potential barrier. For the S_0 potential, there are three doublets below the barrier with torsional states labeled $v = 0, 1$ or 2 , according to increasing eigenenergies, and $+$ or $-$ depending on the symmetry of the corresponding eigenfunction. In the S_1 potential,

²In former calculations (see ref. [61, 126, 127, 128, 129]) the hydrogens of the phosphino group were allowed to relax along ϕ to maintain the local symmetry of the phosphino group. The potential energy curve of the electronic ground state was calculated at the MP2/6-311G(2p,d) level of theory.

the eigenstates are just labeled by ν , implying + or – symmetries for even and odd values of ν .

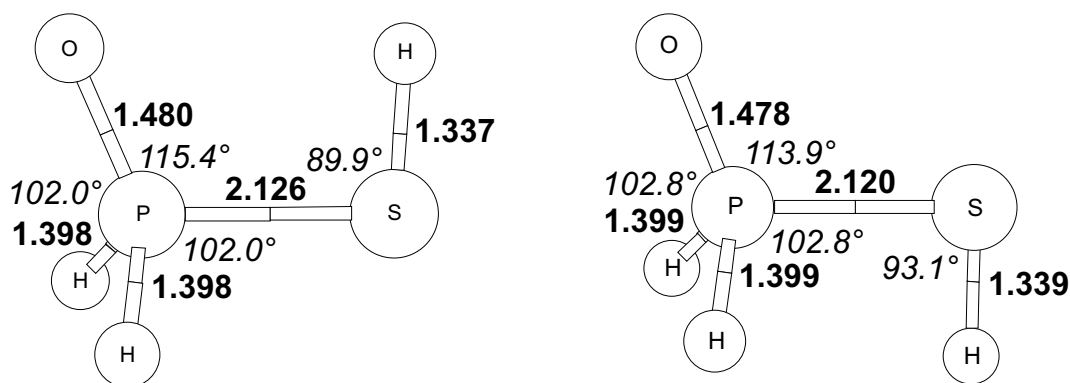


Figure 4.3: Geometries of the *cis*- (left) and *trans*- (right) conformation of H₂POSH optimized at MP2/6-311G(2d,p) level of theory. Bond lengths are given in Ångströms; the angles next to the P-H bonds are measured along HPS.

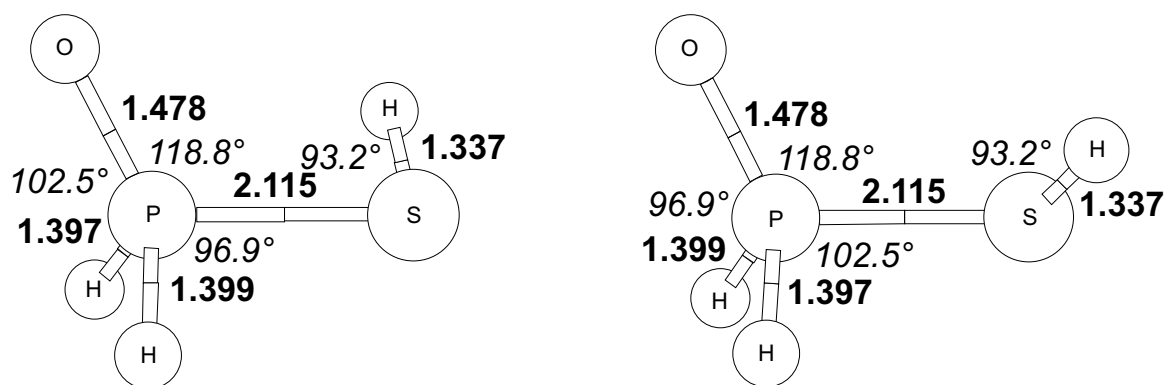


Figure 4.4: Geometries for the *L* (left) and *R* (right) configuration of H₂POSH optimized at MP2/6-311G(2d,p) level of theory. Bond lengths are given in Ångströms; the angles next to the P-H bonds are measured along HPS. The corresponding *symmetric* geometry the P-H bond distances are 1.398 Å and the HPS angles are 99.7°.

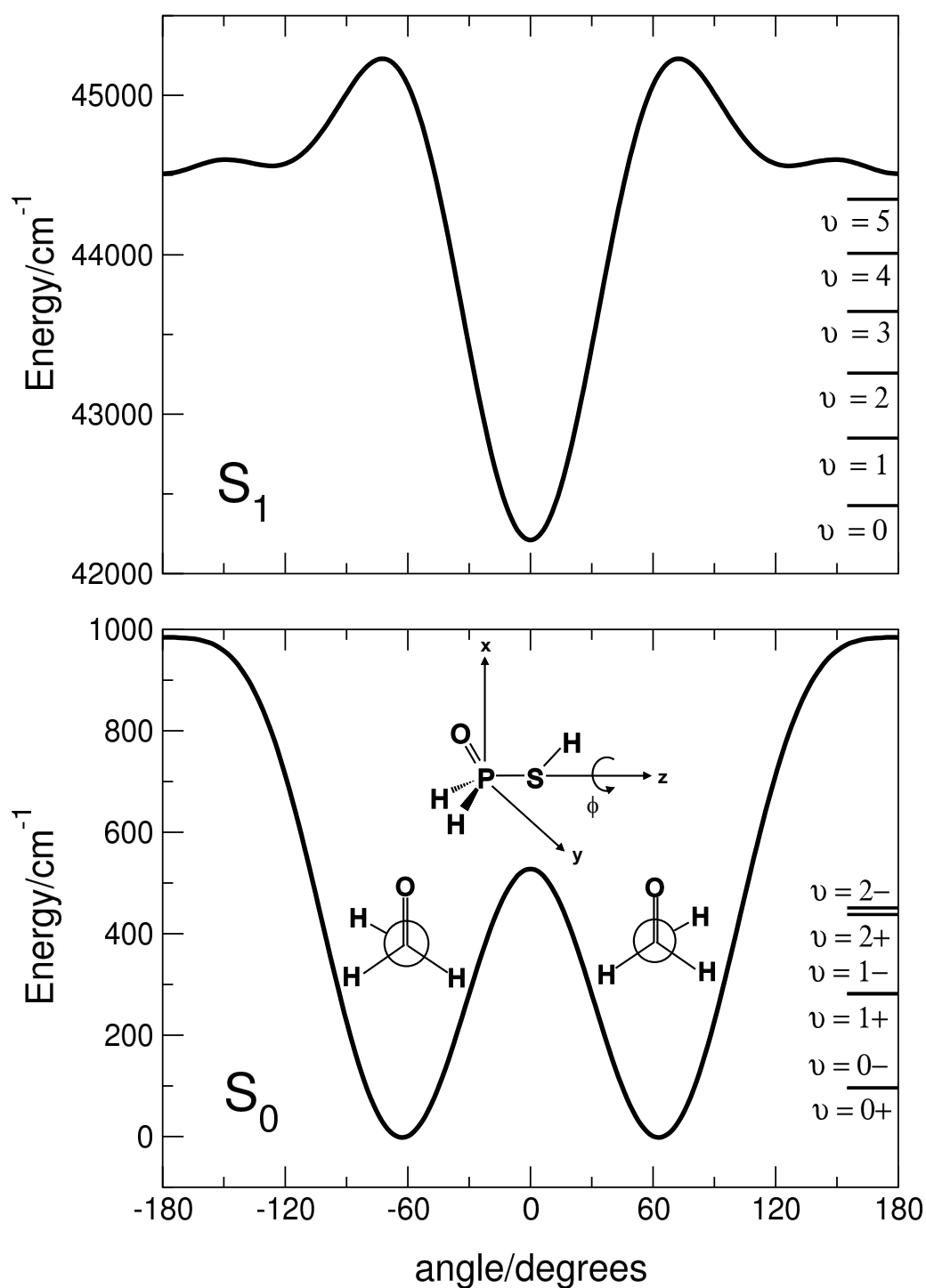


Figure 4.5: The model system H_2POSH with its ground state S_0 and first singlet excited state S_1 potential energy curves (V_i) along the torsional i.e. OPSH dihedral angle (ϕ). $\phi = 0^\circ$ and $\phi = \pm 180^\circ$ correspond to the *cis*- and *trans*-conformations, respectively. Torsional levels for each potential are shown on the right. (adapted from [125])

A CIS/6-311+G(2d,p) optimization of the minimum energy configuration of the molecule in the S₁ state, confirmed by a normal mode analysis, was performed in order to check the geometrical changes induced after electronic excitation of the molecule. A significant elongation of the P-S bond from 2.12 Å in S₀ to 2.81 Å in S₁ was found. This is an indication for a weakly bounded relaxed excited singlet state involving electrostatic and/or polarization interactions between the H₂PO and SH fragments.³ This result, together with the fact that the S₁ wave function is composed of Rydberg transitions from the lone pairs of the oxygen and sulfur to the phosphorus atom, calls for the use of diffuse functions in the basis set. Therefore, the augmented basis set 6-311+G(2d,p) has been used in all the *ab initio* calculations⁴.

The dipole moment of the molecule in the electronic ground state $\vec{\mu}^{00}(\phi)$ as well as the electronic transition dipole moment between S₀ and S₁, $\vec{\mu}^{01}(\phi)$ are calculated using (TD)-DFT with the same functional (B3LYP) and split-valence basis set (6-311+G(2d,p)) as for the PES. The components $\mu_x^{00}(\phi)$, $\mu_y^{00}(\phi)$ and $\mu_z^{00}(\phi)$ of the permanent dipole moment are shown in figure 4.6, the ones of the transition dipole moment $\mu_x^{01}(\phi)$, $\mu_y^{01}(\phi)$ and $\mu_z^{01}(\phi)$ in figure 4.7. The respective components are plotted versus the torsional angle ϕ and are either symmetric or anti-symmetric with respect to the OPS mirror plane, i.e. with respect to $\phi = 0^\circ$. While μ_x^{00} , μ_z^{00} and μ_y^{01} are symmetric with respect to $\phi = 0^\circ$, μ_y^{00} , μ_x^{01} and μ_z^{01} are anti-symmetric. The symmetry of the (transition) dipole components is of great importance for the laser control with polarized light. In section 4.6.1 it will be explained in detail how the symmetry of the (transition) dipole components influences the selectivity of a laser pulses. The variation of the dipole components along ϕ is large for μ_x^{00} and μ_y^{00} , thus causing strong couplings with the x- and y-components of a polarized laser field, satisfying criterion (e). The z-components of the dipole moment μ_z shows very little variation along ϕ and, therefore, will not be used for laser control. In the case of the transition dipole components the variation along ϕ is rather small (≈ 0.6 Debye) for all three components, but still large enough to allow a reasonable coupling with the laser field.

³More recent calculations using CASSCF(14,12)/ANO-L have proven that the molecule dissociates in the S₁ state into its H₂PO and SH fragments [130]. Two-dimensional unrelaxed calculations taking the elongation of the P-S bond into account are performed currently by M. F. Shibl (FU-Berlin).

⁴in contrast to the 6-311G(2d,p) basis employed in former calculations, see ref. [61, 126, 127, 128, 129].

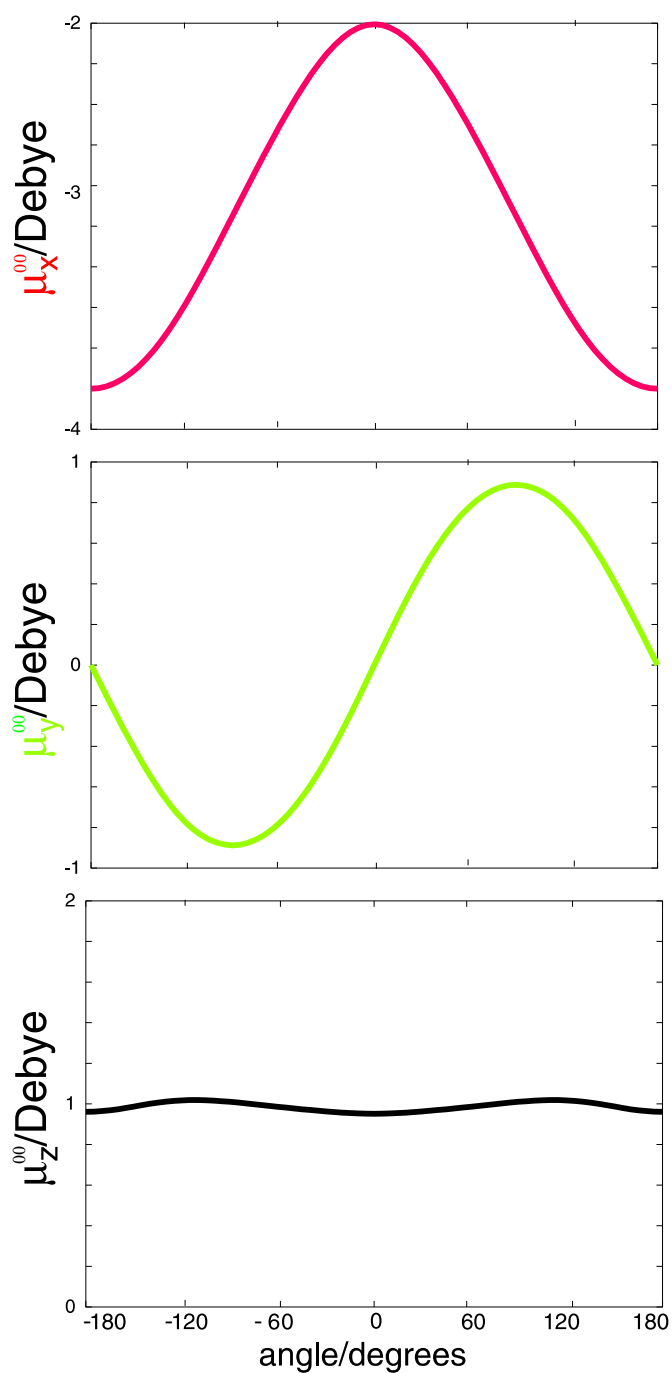


Figure 4.6: Components μ_x^{00} , μ_y^{00} and μ_z^{00} of the permanent dipole moment of H_2POSH versus the torsional angle ϕ (adapted from [127]).

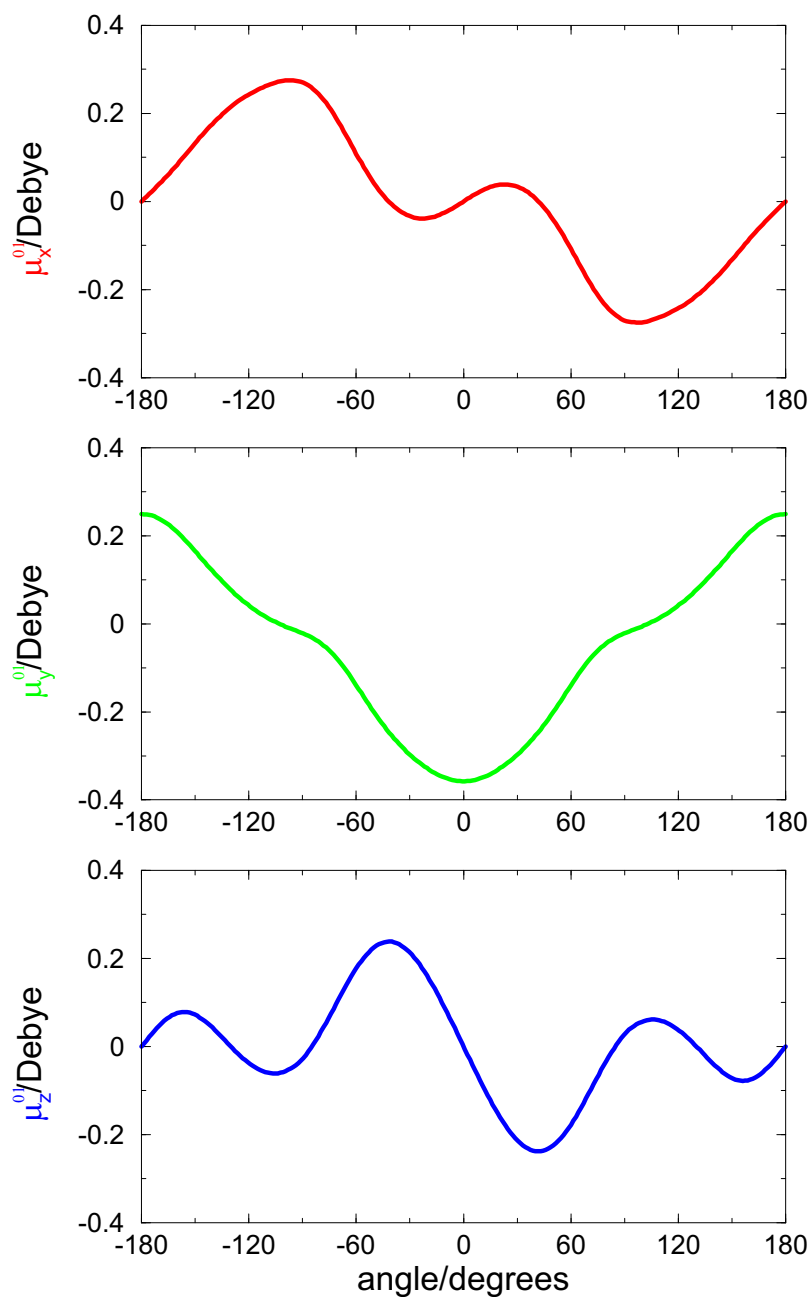


Figure 4.7: Components μ_x^{01} , μ_y^{01} and μ_z^{01} of the electronic transition dipole moment between the electronic states S_0 and S_1 of H₂POSH along the angle ϕ for the torsional motion of the H around the P-S bond (adapted from [125]). (Note that $\mu_y^{01} \approx \mu_z^{01}$ close to the minimum energy configuration at $\phi \approx 60^\circ$, see discussion in section 4.7.2.)

4.4 The Hamiltonian of the 1D model system and its torsional eigenstates

The potential energy curves $V_0(\phi)$ and $V_1(\phi)$ are the basis for the quantum dynamical simulations. In the one-dimensional (1D) model system all degrees of freedom of the H₂POSH molecule are fixed except for the torsional motion of the terminal hydrogen around the P-S bond. This hydrogen is assumed not to affect the atoms of the H₂PO fragment during its rotation. Since the moment of inertia of the H₂PO fragment around the P-S bond is much larger than the one of the SH fragment, as a first approximation the H₂PO fragment is considered to be fixed to its position during the motion of the terminal hydrogen.⁵ Then, the following Hamilton operator can be used to describe the 1D motion:

$$\hat{\mathbf{H}}(\phi) = \hat{\mathbf{T}}(\phi) + \hat{\mathbf{V}}(\phi) = -\frac{\hbar^2}{2I} \frac{\partial^2}{\partial \phi^2} + V(\phi). \quad (4.1)$$

The moment of inertia I is calculated from the mass of the H-atom attached to the sulfur and the perpendicular distance r of this hydrogen to the P-S axis (see figure 4.8):

$$I = m_H r^2 = 1.796 \text{ amu}(\text{\AA})^2 = 11687.87 \text{ m}_e a_0^2$$

$$r = R_{SH} \cdot \sin(180^\circ - \alpha),$$

with $R_{SH} = 1.337 \text{ \AA}$ and $\alpha = 93.16^\circ$.

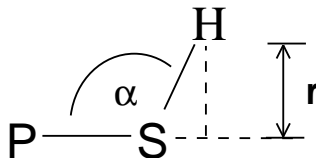


Figure 4.8: Sketch for the calculation of the moment of inertia I

In order to solve equation (4.1) numerically and to obtain the torsional eigenfunctions and eigenenergies the Fourier-Grid-Hamiltonian technique [88, 89] (discussed in section 2.2.8) using a space discretization of 256 grid points was applied by using the program *qmbound* [131]. Figure 4.5 in section 4.3 shows the torsional eigenstates $|\Phi_{v\pm}^0\rangle$ and $|\Phi_v^1\rangle$ of V_0 from $v = 0+$ to $v = 2-$ (in the electronic ground state S_0) and of V_1 for the states $v = 0$ to 5 (in the electronic excited state S_1). The first six torsional eigenfunctions of S_0 are depicted in figure 4.9, the eigenfunctions of S_1 are not shown since their functional

⁵In section 4.6.5 the motion of the H₂PO fragment will be introduced into the model.

behavior is for small v analogous to the eigenfunctions of a harmonic oscillator. In Table 4.1 the exact energies obtained for the first ten torsional states in S_0 (E_{0+}^0 to E_{4-}^0) and in S_1 (E_0^1 to E_9^1) are listed.

S ₀		S ₁	
$E_{v\pm}^0$	eigenvalue [cm ⁻¹]	E_v^1	eigenvalue [cm ⁻¹]
0+	95.9457	0	42426.2
0-	95.9740	1	42850.4
1+	281.144	2	43257.3
1-	282.136	3	43644.3
2+	438.048	4	44009.0
2-	450.910	5	44348.5
3+	558.136	6	44563.5
3-	609.968	7	44619.9
4+	693.026	8	44657.5
4-	767.122	9	44658.5

Table 4.1: Torsional eigenenergies for the electronic ground and first singlet excited state of the model system H₂POSH

As discussed in section 4.3 the potential barrier at $\phi = 0^\circ$ separating the two minima causes an energy splitting of the torsional eigenstates leading to energy doublets below this barrier. For the S_0 potential, there are three doublets $v = 0, 1, 2$ of torsional eigenstates $E_{v\pm}^0$ and torsional eigenfunction $|\Phi_{v\pm}^0\rangle$ with + and - depending on their symmetry with respect to inversion at $\phi = 0^\circ$. The torsional eigenfunctions in the S_1 potential $|\Phi_v^1\rangle$ and their eigenenergies E_v^1 are just labeled by v , implying + or - symmetries for even and odd values of v .

The pure L -enantiomer and R -enantiomer are presented by the localized wave functions $|\Phi_{vL}\rangle$ and $|\Phi_{vR}\rangle$, respectively, embedded in the left and right potential wells of S_0 [30], as shown in figure 4.10. They are constructed as superpositions of two torsional eigenstates in the electronic ground state $|\Phi_{v+}^0\rangle$ and $|\Phi_{v-}^0\rangle$ with + and - symmetry, as defined in eqn. (3.1) (see section 3.4).

The lifetime of a pure enantiomer depends, via the tunneling time, on the energy splitting of the eigenstates within the doublets, see eqn. (3.2). The energy splitting increases with increasing energy since the barrier gets smaller and tighter allowing more interaction between the eigenstates in both wells. In table 4.2 the tunneling times τ_v , defined as the whole oscillation period $L \rightarrow R \rightarrow L$, are listed⁶.

⁶Compare with the values of 630, 20.9 and 1.88 ps respectively obtained with the MP2 potential [61].

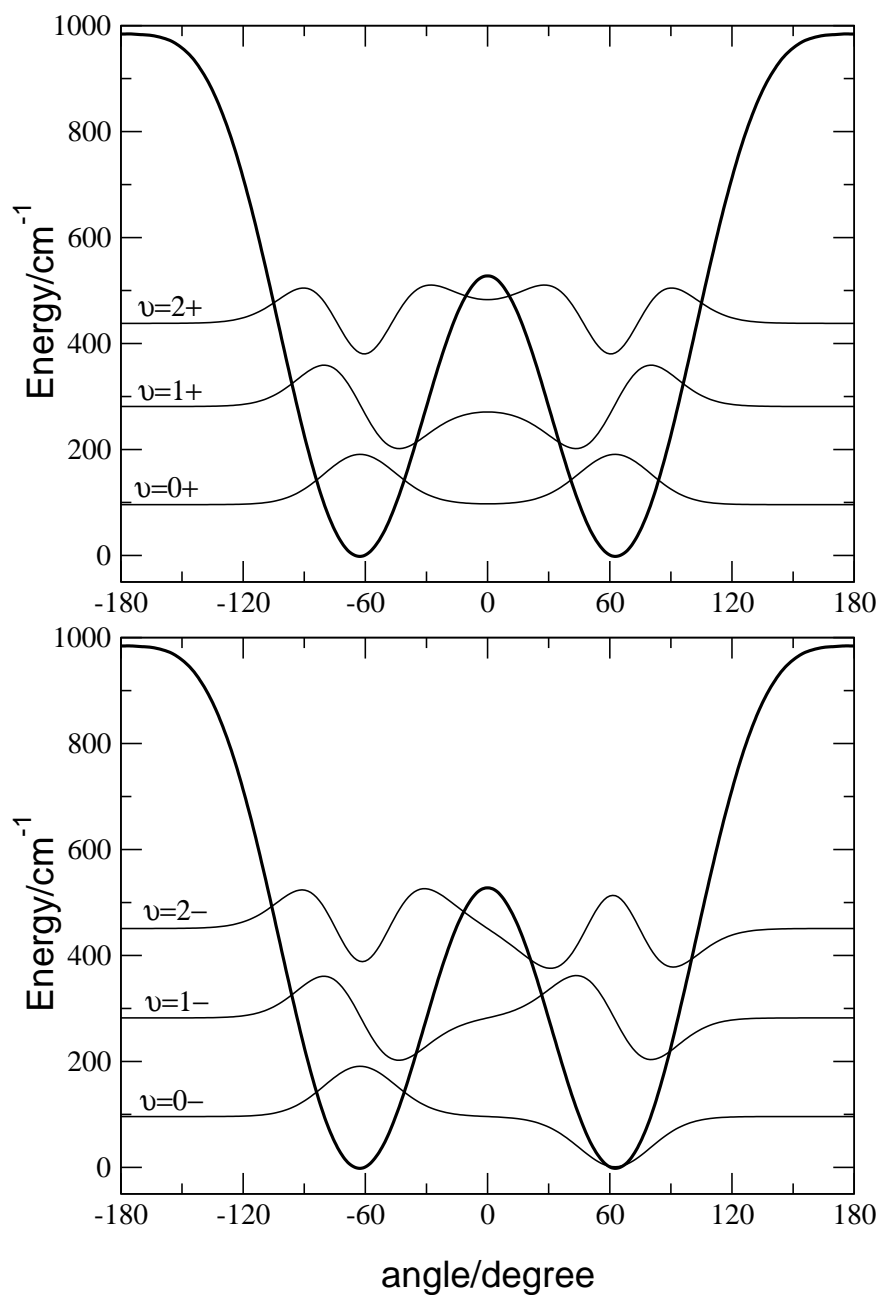


Figure 4.9: Torsional eigenfunctions $|\Phi_{0+}^0\rangle$ to $|\Phi_{2-}^0\rangle$ in the electronic ground state of H₂POSH; with + symmetry: $|\Phi_{0+}^0\rangle$, $|\Phi_{1+}^0\rangle$, $|\Phi_{2+}^0\rangle$ (top panel), and with - symmetry: $|\Phi_{0-}^0\rangle$, $|\Phi_{1-}^0\rangle$, $|\Phi_{2-}^0\rangle$ (bottom panel). Their eigenenergies are indicated by the lines at $\phi = \pm 180^\circ$.

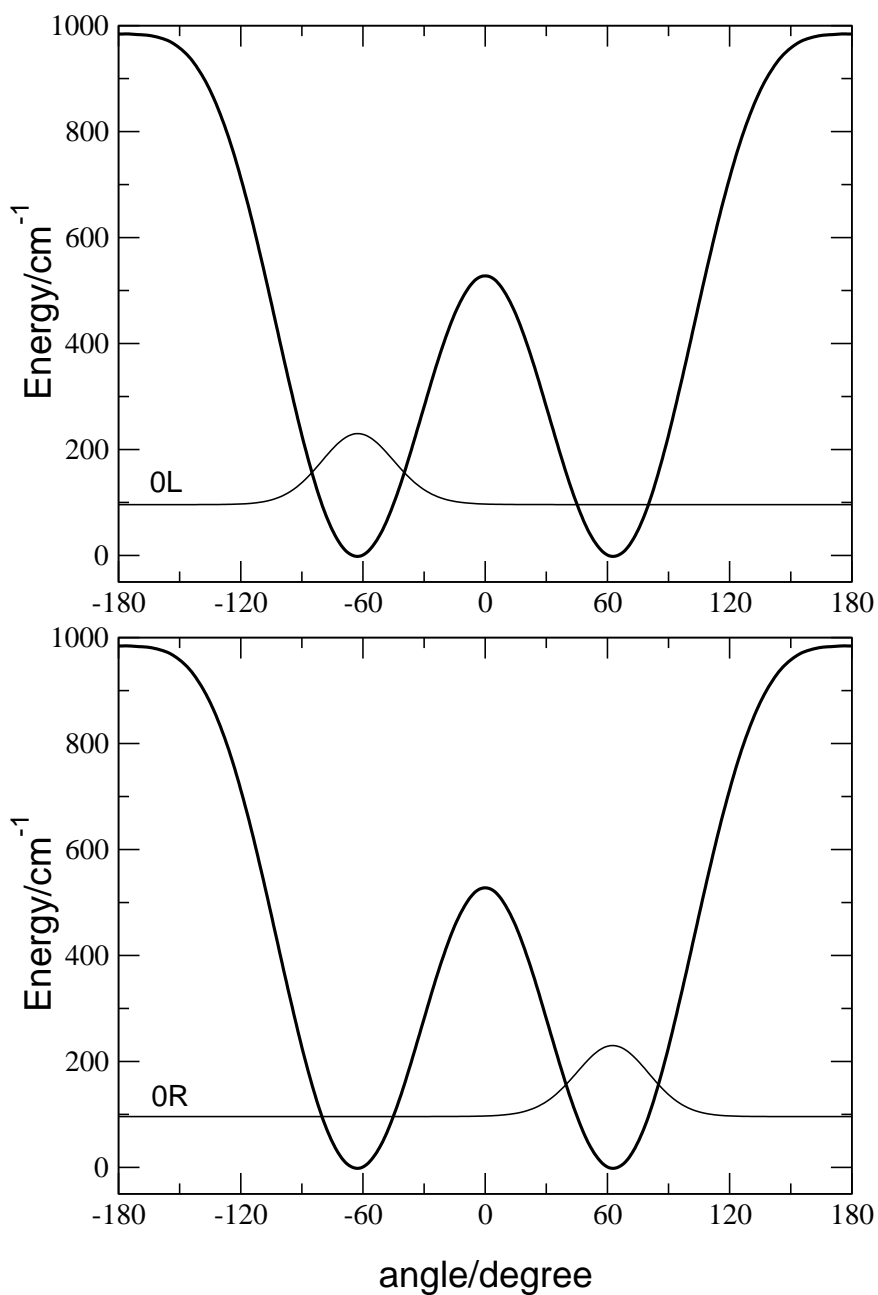


Figure 4.10: Localized wave functions $|\Psi_{0L}\rangle$ and $|\Psi_{0R}\rangle$ of H₂POSH, as defined in eqn. (3.1). $|\Psi_{0L}\rangle$ (top panel) describes the pure *L*-enantiomer in the energetically lowest doublet of the torsional eigenstates $|\Phi_{0+}^0\rangle$ and $|\Phi_{0-}^0\rangle$, cf. fig. 4.9; $|\Psi_{0R}\rangle$ (bottom panel) describes the respective pure *R*-enantiomer.

doublet ν	ΔE_ν^0 [cm ⁻¹]	τ_ν [ps]
0 + /0-	0.0283	1180
1 + /1-	0.992	33.6
2 + /2-	12.9	2.59

Table 4.2: Energy splitting of the doublets ν and the resulting tunneling times τ_ν

The tunneling times are important for the laser control mechanism. If, for example, for the preparation of a pure enantiomer the third doublet $|\Phi_{2\pm}^0\rangle$ is used as intermediate state, the wave packet in this intermediate state will tunnel within 1.29 ps from one well to the other. Hence, a laser pulse that transfers the population from this intermediate state to the final state must be shorter than the lifetime of the localized wave packet in $|\Phi_{2\pm}^0\rangle$ to prevent that the localization is lost. In the following sections, different mechanisms to prepare pure enantiomers will be presented giving more detailed informations about the role of the tunneling times.

4.5 Laser driven dynamics

4.5.1 The time-dependent Hamiltonian

All quantum dynamical simulations that describe an ensemble of distinguishable molecules, i.e. a mixture of enantiomers, are based on the solution of the Liouville-von Neumann equation for the time dependent density matrix $\rho(t)$ of the wave function:

$$i\hbar \frac{\partial \rho(t)}{\partial t} = [H(t), \rho(t)]. \quad (4.2)$$

The time dependent Hamilton operator is given by

$$H(t) = \begin{pmatrix} \hat{\mathbf{T}} + V_0(\phi) - \vec{E}(t) \cdot \vec{\mu}^{00}(\phi) & -\vec{E}(t) \cdot \vec{\mu}^{01}(\phi) \\ -\vec{E}(t) \cdot \vec{\mu}^{01}(\phi) & \hat{\mathbf{T}} + V_1(\phi) - \vec{E}(t) \cdot \vec{\mu}^{11}(\phi) \end{pmatrix}, \quad (4.3)$$

where $\hat{\mathbf{T}}$ is the kinetic energy operator, and $V_0(\phi)$ and $V_1(\phi)$ are the ground and excited molecular potentials, respectively. The coupling with the laser field is treated in the semi-classical dipole approximation including the dipole moments $\vec{\mu}^{ii}(\phi)$ of the electronic states S_0 and S_1 ⁷ and the electronic transition dipole moment $\vec{\mu}^{ij}(\phi)$. In cases where

⁷Since *unrelaxed* potential energy curves are employed $\vec{\mu}^{11}$ is set equal to $\vec{\mu}^{00}$.

only the electronic ground state S_0 is considered, the Hamiltonian $H(t)$ simplifies to $\hat{\mathbf{T}} + V_0(\phi) - \vec{E}(t) \cdot \vec{\mu}^{00}(\phi)$.

4.5.2 Initial state – Final state

The initial density at time $t = 0$ is given by a thermal Boltzmann distribution

$$\rho(t = 0) = \rho(T) = \begin{pmatrix} \rho_{00}(T) & 0 \\ 0 & \rho_{11}(T) \end{pmatrix}, \quad (4.4)$$

where the density of the electronic ground state ρ_{00} is given as

$$\rho_{00}(T) = \sum_v |\Phi_{v\pm}^0\rangle \frac{\exp(-E_{v\pm}^0/k_B T)}{Q} \langle \Phi_{v\pm}^0|, \quad (4.5)$$

with Q being the partition function and k_B the Boltzmann constant. The density ρ_{00} is composed of the densities of the localized torsional eigenstates with energies below the barrier, and those of the delocalized states above the barrier, see eqn. (3.5):

$$\rho_{00}(T) = \sum_{v=0}^2 |\Phi_{v\pm}^0\rangle \frac{\exp(-E_{v\pm}^0/k_B T)}{Q} \langle \Phi_{v\pm}^0| + \sum_{v \geq 3} |\Phi_{v\pm}^0\rangle \frac{\exp(-E_{v\pm}^0/k_B T)}{Q} \langle \Phi_{v\pm}^0|. \quad (4.6)$$

Because the splitting of the doublets is much smaller than the energy differences between two doublets the exact eigenenergies $E_{v\pm}^0$ of the states $|\Phi_{v\pm}^0\rangle$ can be approximated by the average energies \tilde{E}_v^0 of the enantiomer states defined in eqn. (3.1). Then, the densities of the localized torsional states below the barrier $|\Phi_{v\pm}^0\rangle$ can be written in terms of the densities of localized L - and R -wave functions $|\Phi_{vL/R}\rangle$, cf. eqn. (3.6):

$$\begin{aligned} \rho_{00}(T) &\approx \sum_{v=0}^2 |\Phi_{vL}^0\rangle \frac{\exp(-\tilde{E}_v^0/k_B T)}{Q} \langle \Phi_{vL}^0| + \sum_{v=0}^2 |\Phi_{vR}^0\rangle \frac{\exp(-\tilde{E}_v^0/k_B T)}{Q} \langle \Phi_{vR}^0| \\ &+ \sum_{v \geq 3} |\Phi_{v\pm}^0\rangle \frac{\exp(-E_{v\pm}^0/k_B T)}{Q} \langle \Phi_{v\pm}^0| \\ &= \rho_{0L}(T) + \rho_{0R}(T) + \rho_{del}(T), \end{aligned} \quad (4.7)$$

For a case of low temperature (say below 40 K) all Boltzmann weights are negligible except those of the energetically lowest doublet $|\Phi_{0\pm}^0\rangle$, which are approximately equally populated since the states are almost energetically degenerate. Using this approximation, the initial state of all calculations at $t = 0$ is defined as the sum of the L - and R -densities,

representing a racemic mixture of the molecular model system:

$$\begin{aligned}
\rho_{00}(T \rightarrow 0) &\approx \frac{1}{2} \left(|\Phi_{0+}^0\rangle \langle \Phi_{0+}^0| + |\Phi_{0-}^0\rangle \langle \Phi_{0-}^0| \right) \\
&= \frac{1}{2} \left(|\Psi_{0L}\rangle \langle \Psi_{0L}| + |\Psi_{0R}\rangle \langle \Psi_{0R}| \right) \\
&= \frac{1}{2} \rho_{0L}(T) + \frac{1}{2} \rho_{0R}(T).
\end{aligned} \tag{4.8}$$

The density of the electronic excited state ρ_{11} is zero at the initial time. With this initial state the solution of the Liouville-von Neumann equation (4.2) can be written in terms of an incoherent mixture of two time dependent densities

$$\begin{aligned}
\rho(t) &= \frac{1}{2} \left(|\Psi_{0+}(t)\rangle \langle \Psi_{0+}(t)| + |\Psi_{0-}(t)\rangle \langle \Psi_{0-}(t)| \right) \\
&= \frac{1}{2} \left(|\Psi_{0L}(t)\rangle \langle \Psi_{0L}(t)| + |\Psi_{0R}(t)\rangle \langle \Psi_{0R}(t)| \right)
\end{aligned} \tag{4.9}$$

where

$$|\Psi_{0\pm}(t)\rangle = \begin{pmatrix} |\Psi_{0\pm}^0(t)\rangle \\ |\Psi_0^1(t)\rangle \end{pmatrix} \tag{4.10}$$

is a vector composed of the wave function for the electronic ground state $|\Psi_{0\pm}^0(t)\rangle$ and for the electronic excited state $|\Psi_0^1(t)\rangle$, starting from the initial state

$$|\Psi_{0\pm}(t=0)\rangle = \begin{pmatrix} |\Phi_{0\pm}^0(\phi)\rangle \\ 0 \end{pmatrix}, \tag{4.11}$$

with either + or – parity, respectively, whereas

$$|\Psi_{0L/R}(t)\rangle = \begin{pmatrix} |\Psi_{0L/R}^0(t)\rangle \\ |\Psi_0^1(t)\rangle \end{pmatrix} \tag{4.12}$$

is the corresponding vector of the localized L - or R -wave functions, starting from the initial state

$$|\Psi_{0L/R}(t=0)\rangle = \begin{pmatrix} |\Psi_{0L/R}^0(\phi)\rangle \\ 0 \end{pmatrix}, \tag{4.13}$$

with either L or R , respectively. These vectors $|\Psi_{0\pm}(t)\rangle$ or $|\Psi_{0L/R}(t)\rangle$ are solutions of the TDSE:

$$i\hbar \frac{\partial}{\partial t} |\Psi_{0\pm}(t)\rangle = H(t) |\Psi_{0\pm}(t)\rangle \quad \text{or}, \tag{4.14}$$

$$i\hbar \frac{\partial}{\partial t} |\Psi_{0L/R}(t)\rangle = H(t) |\Psi_{0L/R}(t)\rangle. \tag{4.15}$$

Therefore, the solution of the original ansatz using the Liouville-von Neumann equation can be simplified by solving the TDSE either in the basis of torsional eigenstates (4.14)

starting from a 50%:50% incoherent superposition of the states $|\Phi_{0+}^0\rangle$ and $|\Phi_{0-}^0\rangle$, or of the localized L - and R -states starting from a 50%:50% incoherent superposition of the states $|\Psi_{0L}\rangle$ and $|\Psi_{0R}\rangle$.

The final state or target state of the laser driven dynamics is designed either as the pure L - or pure R -enantiomer:

$$\begin{aligned}\rho(t = t_f) &= \sum_{v=0}^2 |\Psi_{vL}\rangle P_{vL}(t_f) \langle \Psi_{vL}| = \rho_L \quad \text{or} \\ \rho(t = t_f) &= \sum_{v=0}^2 |\Psi_{vR}\rangle P_{vR}(t_f) \langle \Psi_{vR}| = \rho_R.\end{aligned}\tag{4.16}$$

To accomplish this, a laser pulse sequence must be designed to convert the initial racemate selectively and if possible completely, i.e. by 100%, into the desired L - or R -enantiomer ($\sum_{v=0}^2 P_{vL}(t_f) \rightarrow 1$ or $\sum_{v=0}^2 P_{vR}(t_f) \rightarrow 1$). Here, it is important to note that no laser control can be designed to localize a racemic mixture exclusively in the lowest doublet, i.e. the target density $|\Psi_{0L}\rangle 1 \langle \Psi_{0L}|$ or $|\Psi_{0R}\rangle 1 \langle \Psi_{0R}|$ cannot be reached starting from the initial state (4.8). This restriction is based on the fact that the maximum value of the population in the target state at time t_f cannot exceed the maximum value of the initial population distribution $\rho(t = 0)$ in a control system without any dissipative process, as shown by Gross *et al.* [132]. Hence, a target state involving not only ground $v = 0$ but also excited doublets $v = 1, 2$ has to be chosen, as specified in eqn. (4.16).

Since not only the energetically lowest doublet, but also excited doublets are populated at final time t_f , the lifetime of the prepared pure enantiomer will also depend on the tunneling times of these excited doublets. The energy splitting of the lowest doublet $|\Phi_{0\pm}^0\rangle$ is 0.0283 cm^{-1} which corresponds to a tunneling time of 1180 ps for a pure enantiomer localized only in this doublet (see table 4.2). This time is long enough for spectroscopically monitoring the pure enantiomer in an experiment fulfilling criterion (e) from section 4.2. The tunneling times for the next higher doublet is 33.6 ps, hence, the part of the wave function localized in this doublet will tunnel in 16.8 ps to the other well causing a partial racemization of the pure enantiomer. For the doublet $v = 2$ the energy splitting is already 12.9 cm^{-1} causing a tunneling time of 2.59 ps; this results in a very short lifetime of the corresponding enantiomer $|\Psi_{2R/L}\rangle$ making the spectroscopically monitoring more difficult. Therefore, an adequate target state should, in case of the here presented model system, include only the doublets $v = 0$ and $v = 1$, i.e. the density at final time should be $\frac{1}{2}\rho_{0L} + \frac{1}{2}\rho_{1L}$. Figure 4.11 shows the initial and the desired final state (here, as an example, the pure L -enantiomer).

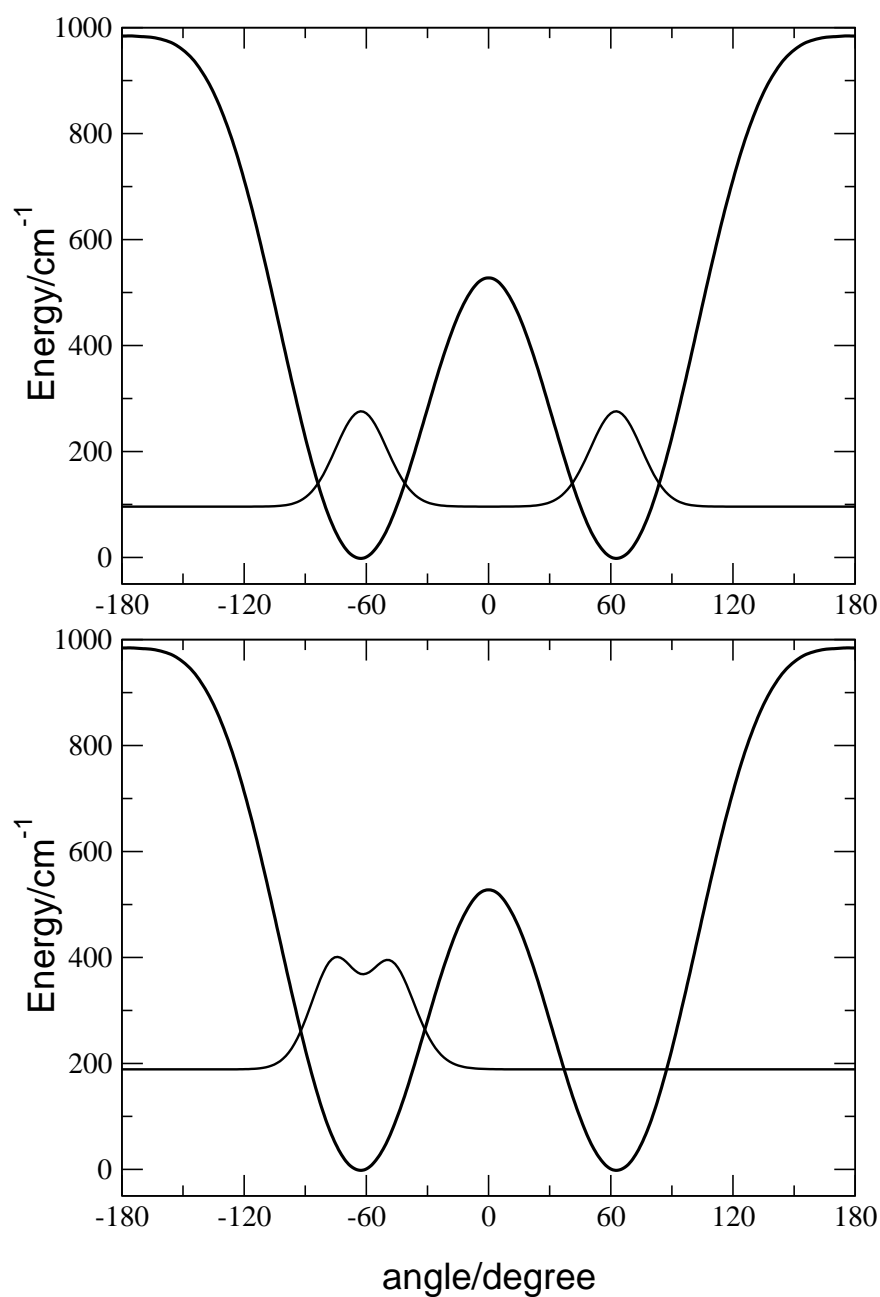


Figure 4.11: The initial state $\frac{1}{2}\rho_{0L} + \frac{1}{2}\rho_{0R}$ at time $t = 0$ (top) presenting a incoherent 50%:50% mixture of both enantiomers forming a racemate, and the desired final state $\frac{1}{2}\rho_{0L} + \frac{1}{2}\rho_{1L}$ at final time t_f corresponding to a pure L -enantiomer (bottom).

Throughout this work the localizations of the time-dependent wave function on the L - or R -states $P_{vL/R}$ of S_0 and the corresponding laser driven populations of the torsional eigenstates $P_{v\pm}^i$ are given by

$$P_{vL/R}(t) = \left| \langle \Psi_{vL/R} | \Psi_{0\pm}^0(t) \rangle \right|^2 \quad (4.17)$$

and

$$P_{v\pm}^i(t) = \left| \langle \Phi_{v\pm}^i | \Psi_{0\pm}^i(t) \rangle \right|^2, \quad (4.18)$$

respectively.

The laser driven dynamics are simulated by wave packet propagations applying the split operator (see section 2.3.2) as implemented in the program *qmpropa* [133]. The propagations were carried out on a grid of 256 points (see section 2.3.1) in time steps of $\Delta t = 0.25$ fs, or $\Delta t = 0.1$ fs if the electronic excited state was included into the calculations.⁸

In the following sections, different laser control mechanisms for the purification of a racemate are described for the one-dimensional model system H₂POSH. Extensions of the model system, taking overall rotations of the molecule into account as well as a possible experimental proof of the successful preparation of pure enantiomers by laser pulses are also discussed.

4.6 The “parking” mechanism

4.6.1 Selective preparation of a localized wave packet

The first simulation of a quantum model system, i.e. H₂POSH, demonstrating the selective preparation of a pure enantiomer by ultra-short laser pulses starting from a racemic mixture was presented by Fujimura *et al.* in [128]. The laser control used in ref. [128] is based on the so-called *parking mechanism*. The mechanism was historically derived from previous work by Fujimura *et al.* [61] using the local control method as well as by González *et al.* [127] using analytical laser pulses. In both references the simulations started from a *coherent* superposition of the L - and R -enantiomers corresponding to the pure torsional ground state $|\Phi_{0+}\rangle$, which is, strictly speaking, not equivalent to a racemic mixture. However, the careful analysis of the enantio-selective laser control achieved by

⁸In either case, smaller time steps did not affect the calculated results.

the local control method allowed to derive several control mechanisms based on analytical laser pulses (for a detailed discussion see refs. [127, 126]). Further investigations by Leal *et al.* [129] on the deuterated species H₂POSD gave a better insight into the effect of the tunneling times for intermediate states and introduced a simplified control scheme that is partly used in the here presented parking mechanism. In the following, first this simplified mechanism will be briefly discussed; then, the parking scheme is introduced.

Probably the simplest way to convert the pure state $|\Phi_{0+}\rangle$, corresponding to a *coherent* superposition of *L*- and *R*-enantiomers, into the localized state $|\Psi_{0L/R}\rangle$ corresponding to a pure *L*- or *R*-enantiomer, using linearly polarized laser pulses is the pump-dump scheme depicted in figure 4.12. The pump pulse induces a transition from the initial state $|\Phi_{0+}^0\rangle$ to an intermediate state, here $|\Phi_{2-}^0\rangle$, transferring only half of the initial population. The subsequent dump pulse deexcites the population from the intermediate state to the other state of the energetically lowest doublet $|\Phi_{0-}^0\rangle$, thus forming selectively the target localized state, here $|\Psi_{0L}\rangle$.

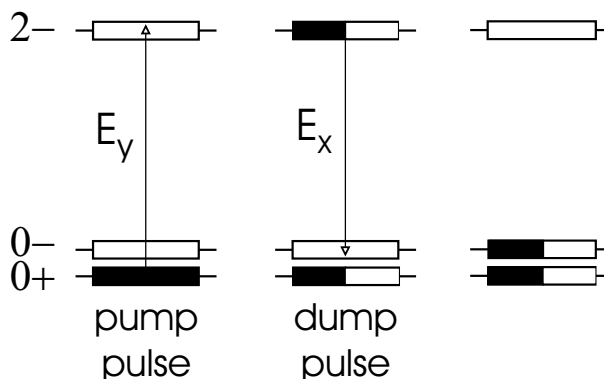


Figure 4.12: Selective transitions of a simple pump-dump scheme for the preparation of the localized state $|\Psi_{0L}\rangle$ starting from an initial pure state $|\Phi_{0+}^0\rangle$ via the intermediate state $|\Phi_{2-}^0\rangle$, using linearly polarized laser pulses (see ref. [129]). The 100% or 50% populations of the states $v\pm$ ($\hat{=}$ $|\Phi_{v\pm}^0\rangle$) are denoted by half and complete filled boxes, respectively.

Both subpulses in fig. 4.12 are linearly polarized, but their polarization vectors are orthogonal to each other. Each subpulse connects two states of specific symmetry obeying the selection rules. The selection rule determines a transition to be *allowed* if the squared absolute value of the transition dipole moment vector $\vec{\mu}_{vv'}$ is unequal zero:

$$\vec{\mu}_{vv'} = \langle \Phi_v | \vec{\mu} | \Phi_{v'} \rangle, \quad |\vec{\mu}_{vv'}|^2 \neq 0. \quad (4.19)$$

If the condition (4.19) is not fulfilled the corresponding transition cannot be induced by a laser pulse and this transition is said to be *forbidden*. Since the molecule is considered

to be fixed in space the (transition) dipole moment can only undergo changes along the torsional degree of freedom. Thus, the components of the (transition) dipole moment μ_x^{00} , μ_y^{00} and μ_z^{00} (see fig. 4.6), or for electronic transitions μ_x^{01} , μ_y^{01} and μ_z^{01} (see fig. 4.7), respectively, are either symmetric or anti-symmetric with respect to inversion at $\phi = 0^\circ$. Hence, depending on the symmetry of eigenstates involved in the transition only certain polarization directions of the laser field are able, i.e. allowed in terms of the selection rule (4.19), to induce the transfer of population.

Following the selection rules the first transition shown in figure 4.12 must be coupled by a dipole moment component with $-$ symmetry since the affected states $|\Phi_{0+}^0\rangle$ and $|\Phi_{2-}^0\rangle$ are of different symmetry. For the same reason the second pulse, the dump pulse, has to be coupled to a dipole moment component with $+$ symmetry since the affected states $|\Phi_{2-}^0\rangle$ and $|\Phi_{0-}^0\rangle$ are of the same symmetry. Looking at the dipole moment components of H₂POSH in fig. 4.6 one realizes that the pump pulse must be y-polarized while the dump pulse must be x-polarized for a laser propagating in z-direction.

The sequence of laser pulses used in the simulation together with the laser parameters, the resulting population dynamics and localization of the wave packet are illustrated in figure 4.13. The first linearly polarized pulse, $E_y(t)$, transfers close to 50% of the population of the initial state $|\Phi_{0+}^0\rangle$ to $|\Phi_{2-}^0\rangle$ whereas the second pulse, $E_x(t)$, deexcites the population of $|\Phi_{2-}^0\rangle$ to $|\Phi_{0-}^0\rangle$, thus forming the target localized state $|\Psi_{0L}\rangle$.

The amount of localization of the target state $|\Psi_{0L}\rangle$ depends on its tunneling time, on the tunneling time of the intermediate wave packet ($\frac{1}{2}|\Phi_{0+}^0\rangle + \frac{1}{2}|\Phi_{2-}^0\rangle$), on the pulse duration of the dump pulse and on the relative phase $\eta = \eta_x - \eta_y$, i.e. the phase difference between the phase-locked pump and dump pulse. The wave packet which is formed in the energetically lowest doublet during the dump pulse consists of a coherent superposition of the states $|\Phi_{0+}^0\rangle$ to $|\Phi_{0-}^0\rangle$ and, once formed, it starts to tunnel through the central barrier since it is not a stationary state of the system. Therefore, the duration of the dump pulse in comparison with the tunneling time of the prepared localized wave packet influences the level of localization of the wave packet at the end of the pulse. If, for example, the tunneling time is much shorter than the duration of the dump pulse, the prepared wave packet will tunnel back and forth through the barrier a couple of times until the interaction with the laser has ended.

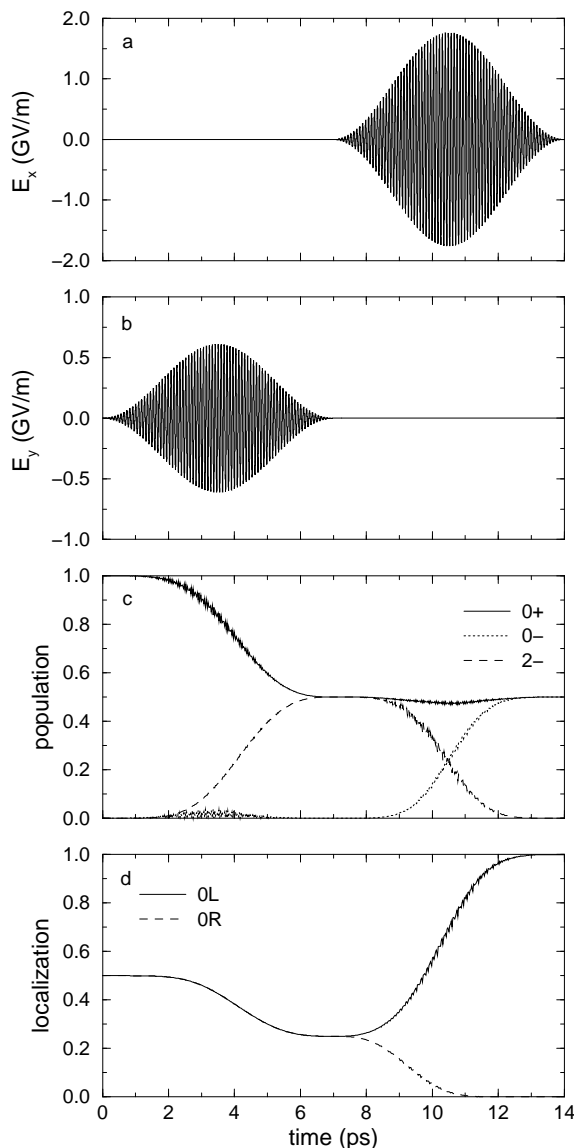


Figure 4.13: Selective preparation of the *L*-enantiomer of H₂POSH by two linearly polarized laser pulses using the pump-dump scheme shown in fig. 4.12. Panel (a) and (b) show the electric field components E_x and E_y . Panel (c) depicts the time-evolution of the population dynamics of the eigenstates involved in the mechanism ($P_{v\pm}^0 \hat{=} v\pm$), and panel (d) shows the time-evolution of the localization as defined in eqn. 4.17 ($P_{vL/R} \hat{=} vL/R$). The laser parameters are $E_y^0 = 0.61$ GV/m, $E_x^0 = 1.76$ GV/m, $\omega_y = 373.36$ cm⁻¹, $\omega_x = 372.70$ cm⁻¹, $\eta_y = 0^\circ$, $\eta_x = 25^\circ$, and the time durations are $t_p = 7$ ps for both pulses. (adapted from ref. [129])

If, on the other hand, the dump pulse is very short compared with the tunneling time, which is true for the here presented model system (1180 ps vs. 7 ps), then the tunneling time of the target doublet has almost no effect on the level of localization⁹. In this case the tunneling time of the intermediate wave packet which has been neglected in the previous discussion becomes important for the localization of the target state. Since the intermediate wave packet is higher in energy than $|\Psi_{0L}\rangle$ its tunneling time is shorter than the one of $|\Psi_{0L}\rangle$ and therefore, its effect on the localization is even bigger than the effect of the tunneling time of $|\Psi_{0L}\rangle$. As mentioned above, the pulse duration of the dump pulse in comparison with the tunneling time, now the one of the intermediate state is considered, defines the amount of localization after the dump pulse. But during the laser interaction the intermediate state $|\Phi_{2-}^0\rangle$ is depopulated and hence, the intermediate wave packet is decreasing in energy and increasing in tunneling time until it reaches the target state. In conclusion all dynamical effects due to the tunneling of the wave packet at a certain time of the control sequence are very difficult to control. In practice, only the relative phase η between the two subpulses is used to affect the localization of the prepared wave packet. If a given pump-dump sequence is creating a wave packet completely localized in one potential well, then the same pulse sequence with a relative phase changed by $\pm\pi$ will produce a wave packet in the other well. Hence, the selectivity of preparing the pure *L*- or *R*-enantiomer can be controlled by optimizing the relative phase η between both pulses. Since the required phase depends on dynamic factors which are difficult to predict for a molecular model system¹⁰, the relative phase has to be optimized by hand for a given pump-dump sequence.

This simple pump-dump scheme to prepare selectively a localized wave packet starting from a pure state is an important step for the parking mechanism introduced in the following section, which is used for the purification of a real racemate, i.e a *incoherent* superposition of the *L*- and *R*-enantiomer.

4.6.2 The structure of the five-step parking scheme

The parking mechanism was derived from previous investigations on the preparation of localized states, eventually allowing the selective purification of a “true” racemic mixture [128]. This, and the following section, will explain the parking mechanism and present results of its application to the H₂POSH model system using different intermediate states in the electronic ground and in the electronic excited state. Different types of laser control using analytical laser pulses, as well as STIRAP are also discussed.

⁹This is true for the energetically lowest doublet, differences for the first excited doublet being a target state will be discussed later.

¹⁰For an approximated approach in case of a three-level Λ system without tunneling see ref. [125].

For the selective preparation of either the pure *L*- or the pure *R*-enantiomer from a racemate the selective transitions induced by the five sequential linearly polarized subpulses of the so-called the “parking” mechanism are illustrated in figure 4.14.

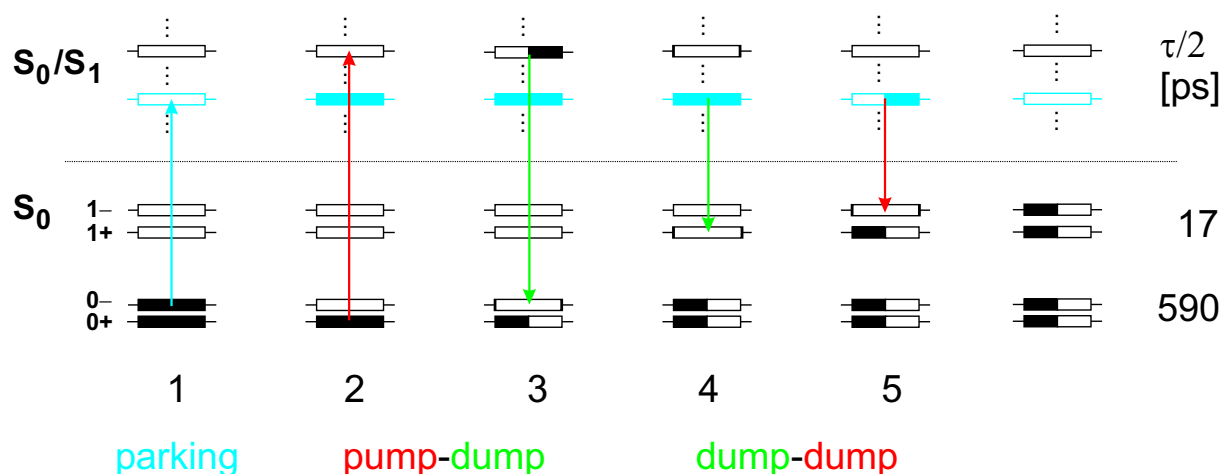


Figure 4.14: Selective transitions between the torsional states v_{\pm} ($\cong |\Phi_{v_{\pm}}^0\rangle$) of the electronic ground state S_0 and intermediate states of either S_0 or the electronic excited state S_1 induced by a sequence of five linearly polarized laser pulses. $\tau/2$ are the life times of the localized states $|\Psi_{vL/R}\rangle$.

The amplitudes of the five subpulses depend, as shown in eqn. (2.99), on the laser pulse duration and on the value of the transition dipole matrix element. In an ideal case, the subpulses transfer either 100% or 50% of the population from one state to another. In case of 100% population transfer the pulses are called π -pulses because their laser parameters can be derived from the π -pulse theory (see section 2.4.1) for two-level systems. If only half of the population is transferred between two states then the laser pulse inducing this transition is called a half- π -pulse. Then, the laser pulse amplitude is about half the value of a π -pulse in the approximation of a two-level system. In any case, π and half- π pulses are used to simplify the problem; in general, every subpulse must be optimized for the “real” molecular multi-level system.

A key step of the mechanism sketched in figure 4.14 is to transfer completely the population of one of the initial states (for instance $|\Phi_{0-}^0\rangle$) to a torsional state higher in energy, the so-called “parking” step. The “parked” population should not be affected by any of the sequential pulses which will follow (steps 2-3). Then, the population in the remaining $|\Phi_{0+}^0\rangle$ state undergoes a pump-dump mechanism (second and third step) by

a sequence of a half- π followed by a π -pulse. These two-pulse sequence is equivalent to the simple pump-dump mechanism discussed in the previous section. First, the half- π -pulse pumps half the population to an intermediate excited state which must be different from the “parking” state. The pump pulse and also the following dump pulse must be optimized in such a way that they do not affect the “parked” population. Next, a π -pulse dumps completely the population in the intermediate state to the unpopulated partner of the lowest doublet, i.e. to the unpopulated state, here $|\Phi_{0-}^0\rangle$, in the lowest doublet of torsional states of S_0 . In this way a coherent superposition of $|\Phi_{0+}^0\rangle$ and $|\Phi_{0-}^0\rangle$ with equal populations is created. The phase of the dump pulse η is chosen such that the wave packet is localized in either the left or in the right well of the double minimum potential curve V_0 [127].

In the fourth and fifth steps the “parked” population is deexcited to create another coherent superposition of torsional states in the first excited doublet of S_0 . Each half of the “parked” population is dumped to the two torsional states of the first excited doublet, $|\Phi_{1+}^0\rangle$ and $|\Phi_{1-}^0\rangle$, thus creating a coherent 50%:50% superposition of $|\Phi_{1\pm}^0\rangle$. This can be done either by a sequential process using a half- π -pulse followed by a π -pulse, or by simultaneous deexcitation via two pulses of different polarization with area equal to π .¹¹ In the former case the area of the pulses for the overall transition is larger (1.5π versus π). In the last case, since both pulses are acting at the same time, the overall transition is faster, but the competing transitions make the process more sensitive to the individual field amplitudes. Again the localization will depend on the choice of the relative phase η between both pulses, in an analogous way as in the second and third steps. In any case, if the wave packets in the lowest and first excited doublets of S_0 are both localized on the same side of the central barrier of S_0 , the localization, as defined in Eq. (4.17), is equal to one. Then the racemate is completely purified, and either the left or the right enantiomer is prepared.

4.6.3 Laser control by means of IR pulses using the “parking” mechanism

The “parking” state (step 1) as well as the intermediate state for the pump-dump sequence (step 2 and 3) can be either a torsional eigenstate in the electronic ground state [128] or a torsional state in the electronic excited state [125]. In Figure 4.15 the result for the

¹¹In the case of simultaneous deexcitation the Rabi frequency of the overall transition is the effective Rabi frequency $\Omega = \Omega_1(t) + \Omega_2(t)$, whose area must be equal to an odd multiple of π for full population transfer. Since we require $\Omega_1(t) = \Omega_2(t)$ for a balanced transfer to both final levels, the areas of each individual pulse must be $A_1 = A_2 = \pi/2$.

“parking” mechanism via torsional states in the electronic ground state is illustrated for the selective preparation of the L -enantiomer from a racemate. The laser parameters of the subpulses shown in figure 4.15 are summarized in table 4.3. At the end of the laser pulse sequence, the total population of the L -enantiomer is close to 1, while the population of the R -enantiomer is close to zero; the remaining small fraction corresponds to the population of delocalized torsional states.

parameter	pulse 1	pulse 2	pulse 3	pulse 4	pulse 5
E_x^0 [GV/m]	0.0	0.0	1.76	0.08	0.0
E_y^0 [GV/m]	1.446	0.611	0.0	0.0	0.17
ω [cm^{-1}]	352.75	373.36	372.7	160.0	161.0
t_p [ps]	7	7	7	7	7
t_d [ps]	0	7	14	21	28
η [degree]	0	0	25	0	180

Table 4.3: Laser parameters of the five subpulses as pictured in fig. 4.15.

The laser field always propagates along the z axis, that is, parallel to the P-S bond of the pre-oriented molecule. Using the techniques discussed previously (see also [134]) the laser field has been constructed from five linearly x - or y -polarized subpulses which in accordance with the symmetry selection rules induce nearly perfect state selective torsional transitions. Specifically, the dipole components μ_x^{00} and μ_y^{00} have + and – symmetry (see fig. 4.6), respectively; thus the interacting linearly x - and y -polarized subpulses induce transitions only between states with identical or opposite symmetries, respectively.

As seen in figure 4.15 the first, y -polarized subpulse transfers almost completely the population of the initial state $|\Phi_{0-}\rangle$ into the excited state $|\Phi_{2+}\rangle$, the “parking” state, without influencing the population of the other initial state $|\Phi_{0+}\rangle$. Next, the second and third y - and x - polarized subpulses transfer the initial population of the other initial state $|\Phi_{0+}\rangle$ into the ground state of the L -enantiomer, $|\Psi_{0L}\rangle$, while leaving the “parked” population of state $|\Phi_{2+}\rangle$ unaffected. This is achieved by first transferring half of the initial population of $|\Phi_{0+}\rangle$ into the excited state $|\Phi_{2-}\rangle$ and subsequently to $|\Phi_{0-}\rangle$, which then interferes coherently with the remaining fraction of $|\Phi_{0+}\rangle$ leading to the formation of the target state of the L -enantiomer $|\Psi_{0L}\rangle$. Finally, the “parked” population of $|\Phi_{2+}\rangle$ is dumped into the excited ($\nu = 1$) state of the L -enantiomer $|\Psi_{1L}\rangle$, by means of the fourth and fifth subpulses which create the corresponding coherent superposition of states $|\Phi_{1+}\rangle$ and $|\Phi_{1-}\rangle$, respectively, without influencing the population of $|\Psi_{0L}\rangle$.

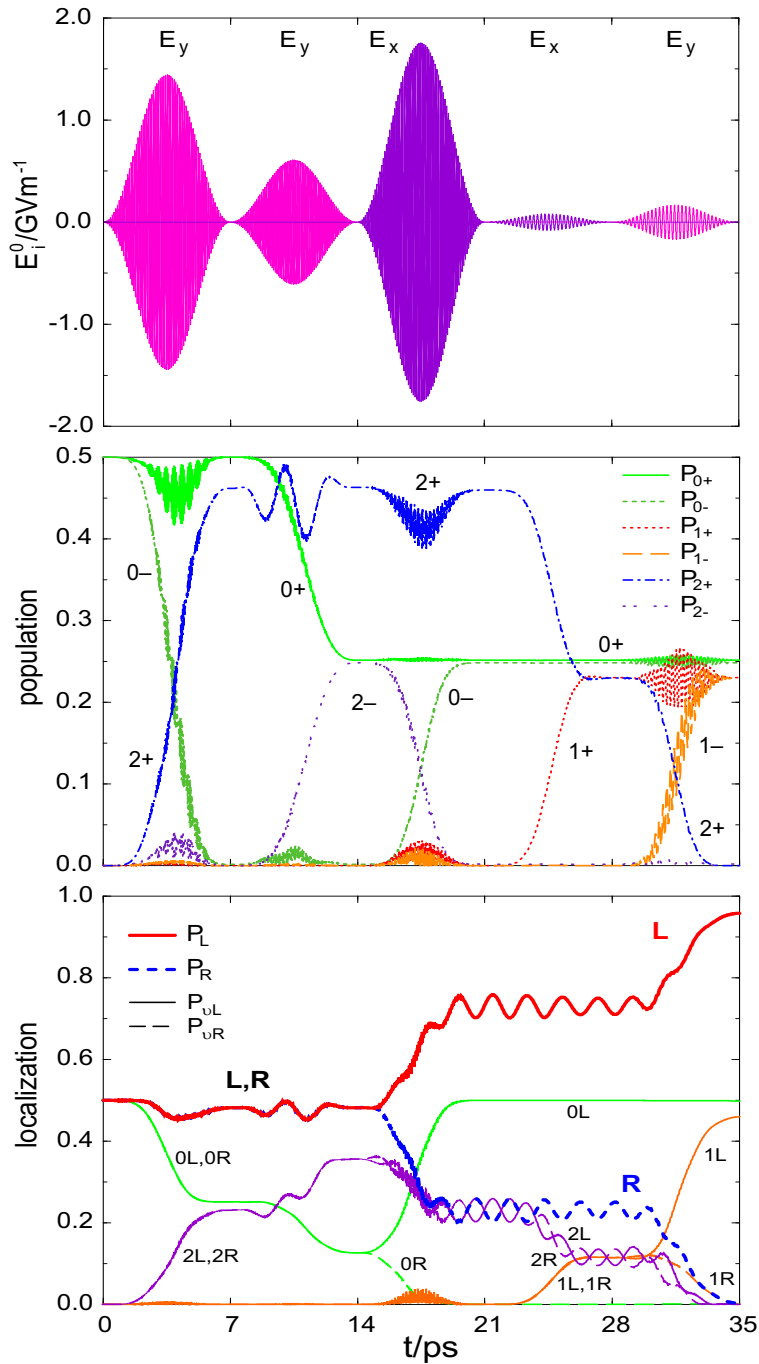


Figure 4.15: Selective preparation of the L -enantiomer from a pre-oriented racemate of the model H₂POSH, by means of a sequence of five linearly polarized laser pulses. Top panel: Electrical field of the linearly x - or y -polarized pulses. Middle panel: Population dynamics of the torsional states $|\Phi_{v\pm}^0\rangle$ (labeled $v\pm$) as induced by the subpulses. Bottom panel: Resulting localized populations P_{vL} and P_{vR} of the doublets $v = 0, 1, 2$ and the total populations P_L and P_R of the L - and R -enantiomer; marginal populations of more excited delocalized levels are not shown. (top and bottom panels are adapted from ref. [128])

The net effect is the conversion of the undesirable *R*-portion of the racemate from its torsional ground state to the *L*-enantiomer in its first torsional excited state, while keeping the initial fraction of the desired enantiomer in its torsional ground state. This is accomplished by converting the incoherent population of two initial states (the racemate) into an incoherent superposition of two coherent states (the *L*-enantiomer), where the coherences in each of the doublets are introduced by the second to fifth subpulses. After the end of the pulses, the pure enantiomer will tunnel back and forth towards the opposite enantiomer. Therefore, the enantiomer selectivity remains only during half of the tunneling time ($\tau_1/2$). This time is long enough, however, for subsequent laser control or reactions which may stabilize the pure enantiomer, see e.g. refs. [52, 49].

Tunneling is also present during the laser pulse, but it will not destroy the final localization because it is exceedingly slow for $|\Psi_{0L}\rangle$ (1180 ps). Moreover, the more rapid tunneling of the wave packet created in the intermediate parking states $|\Phi_{2+/2-}^0\rangle$ as well as in the first excited doublet $|\Phi_{1+/1-}^0\rangle$ was considered by choosing a proper phase for the third and fifth laser pulse (see table 4.3).

4.6.4 Laser control by means of UV pulses

The “parking” state (step 1) as well as the intermediate state for the pump-dump sequence (step 2 and 3) can also be chosen to be torsional eigenstates in the electronic excited state S_1 . Figure 4.16 illustrates the selective preparation of the *L*-enantiomer by a sequence of five linearly polarized π and half- π laser pulses inducing transitions between torsional states in S_0 and S_1 , with the corresponding evolution of the population dynamics and localization dynamics.

The first laser pulse of the sequence shown in fig. 4.16 is the “parking” pulse. In principle, any torsional state of the S_1 state can act as a “parking” state. In practice, however, a clever choice of the “parking” state as well as other intermediate states is needed. This involves a careful examination of the coupling between the torsional eigenstates of S_0 and S_1 , i.e. the matrix elements involving the electronic transition dipole moment $\langle \Phi_v^1 | \vec{\mu}^{01}(\phi) | \Phi_{v\pm}^0 \rangle$, to identify the most optically active transitions, which allow to use lower intensities, avoiding thus other unwanted transitions. It is for this reason that y- and z-linearly polarized pulses are used. The laser pulse parameters of all five subpulses shown in Fig. 4.16 are summarized in table 4.4.

parameter	pulse 1	pulse 2	pulse 3	pulse 4	pulse 5
E_y^0 [GV/m]	0.0	0.0	10.0	2.45	0.0
E_z^0 [GV/m]	11.2	16.0	0.0	0.0	6.80
ω [cm ⁻¹]	43138.5	43580.0	43480.0	42950.0	42965.0
t_p [fs]	750	200	500	500	500
t_d [ps]	0	750	950	1450	1950
η [degree]	0	0	114	0	201

Table 4.4: Laser parameters of the five subpulses as depicted in fig. 4.16

The "parking" pulse transfers completely the population from the state $|\Phi_{0-}^0\rangle$ to $|\Phi_2^1\rangle$. The second and third laser pulses create the first coherent superposition $|\Phi_{0\pm}^0\rangle = |\Psi_{0L}\rangle$ in the lowest doublet of S_0 . The third excited torsional state in S_1 , $|\Phi_3^1\rangle$, is used as an intermediate state for this pump-dump sequence. This intermediate state is energetically higher than the "parking" state to prevent competing transitions which would dump the "parked" population to other excited torsional states of S_0 , for instance above the barrier. This process, population and depopulation of the intermediate state $|\Phi_3^1\rangle$, takes place in less than 1000 fs and in the meantime, the population of the "parking" state is not affected. After the third pulse (≈ 1500 fs) both states $|\Phi_{0+}^0\rangle$ and $|\Phi_{0-}^0\rangle$ are populated almost evenly by 0.25 each. As shown in fig. 4.16 the localization of $|\Psi_L\rangle$ has reached almost 0.75.

The last two pulses will create another coherent superposition in $|\Phi_{1\pm}^0\rangle = |\Psi_{1L}\rangle$. The first pulse induces a 50% transition from the "parking" state $|\Phi_2^1\rangle$ to $|\Phi_{1+}^0\rangle$ state. The second pulse dumps the remaining 50% population from the "parking" state to the state $|\Phi_{1-}^0\rangle$ creating thus a 0.25 to 0.25 superposition in the doublet $|\Phi_{1\pm}^0\rangle$. The localization of the system increases then to almost 1 (cf. Fig. 4.16).

The overall duration of the five laser pulse sequence is less than 2.5 ps, more than a factor 10 shorter in comparison with the IR scheme in the previous section. Using torsional states of the electronic excited state as "parking" states as well as intermediate states in the parking pulse scheme allows to apply much shorter laser pulses, which should compete more efficiently against side effects like IVR than long IR pulses. Furthermore, all transition frequencies are in the UV domain which is experimentally much easier to apply than the IR laser pulses used in the previous simulation.

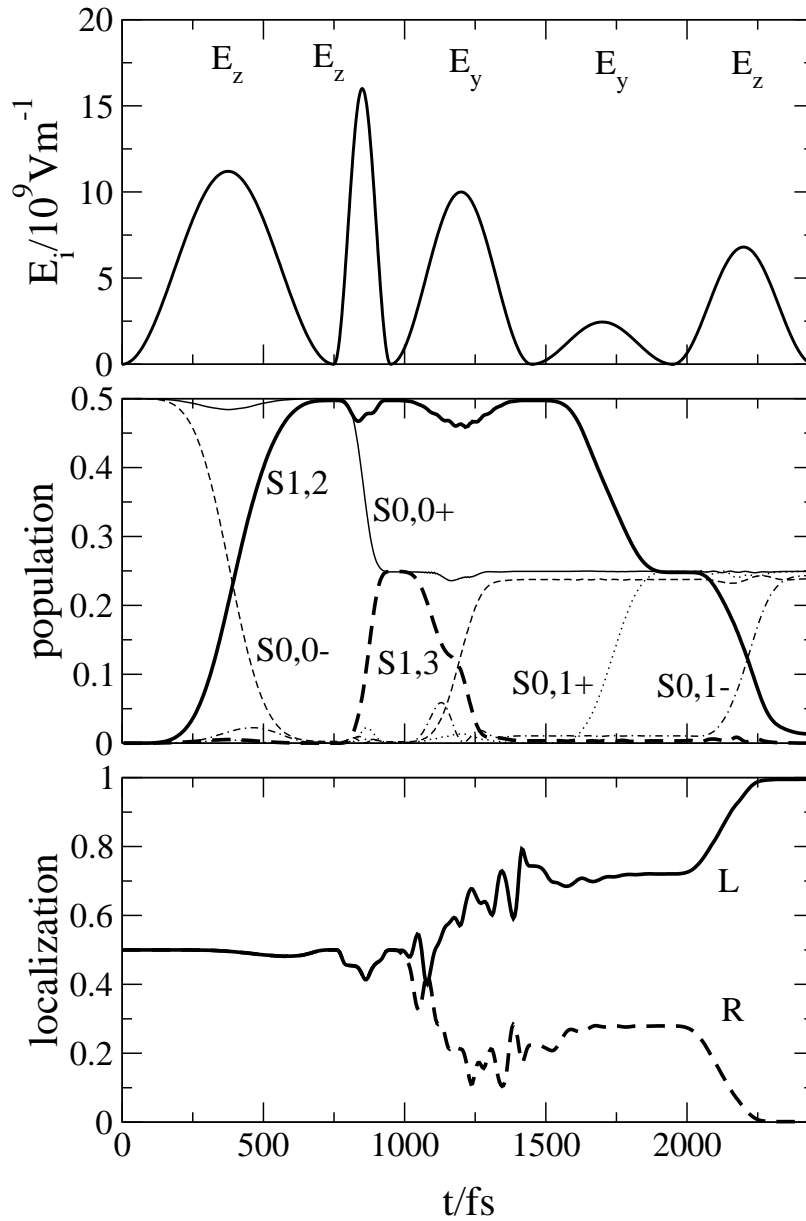


Figure 4.16: Selective preparation of the L -enantiomer using the parking strategy. Top panel: Electric field components E_y and E_z versus time; shown are only the envelope functions. Middle panel: Resulting laser driven population dynamics $P_{v\pm}^i$ as defined in eqn. 4.18, labeled as $S_{i,v\pm}$. Bottom panel: Time evolution of the population, as defined in eqn. 4.17, localized on the left (L /solid line) and right (R /dashed line) sides of the potential. (adapted from ref. [125])

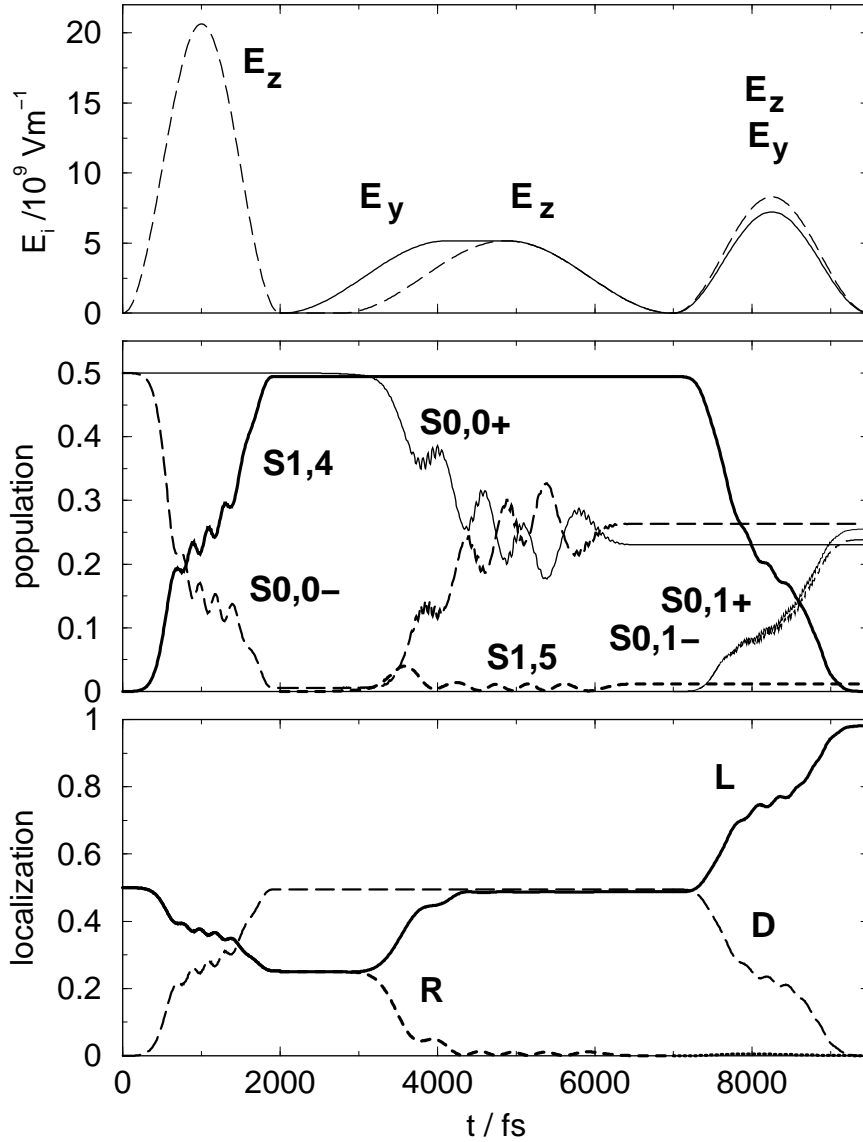


Figure 4.17: Selective preparation of the *L*-enantiomer by an adiabatic strategy based on the parking mechanism. Top panel: Electric field components E_y (solid line) and E_z (dashed line) versus time (only the envelope functions are shown). The pulse parameters are for pulse 1) $E_z^0 = 20.6$ GV/m, $t_p = 2$ ps and $\lambda = 9 \cdot 10^{-9}$ a.u. (approximately $82 \text{ cm}^{-1}/\text{ps}$, see eqn. 2.97), 2) $E_y^0 = E_z^0 = 5.1$ GV/m and $t_{p,y} = t_{p,z} = 4.25$ ps [not including the constant period of 750 fs in $E_y(t)$], 3) $E_y^0 = 7.2$ GV/m and $E_z^0 = 8.26$ GV/m, $t_p = 2.5$ ps and $\lambda = -8 \cdot 10^{-9}$ a.u. ($\sim 73 \text{ cm}^{-1}/\text{ps}$). Middle panel: Resulting laser driven population dynamics $P_{v\pm}^i$ as defined in eqn. 4.18, labeled as $S_{i,v(\pm)}$. Bottom panel: Time evolution of the population, as defined in eqn. 4.17, localized on the left (*L*/solid line) and right (*R*/dashed line) sides of the potential, and in delocalized states (*D*-long dashed line) (adapted from ref. [125]).

The parking mechanism uses pulses with minimum area, such that the theoretical pulse area of the overall process is 4π ¹². This provides results at the shortest possible time or with the lowest intensity requirements. However, population inversion via π -pulses is rather sensitive to the exact value of the pulse area, and therefore, the scheme is not particularly robust under changes in the intensity or time width of the pulses. Hence, a possible extension of the parking mechanism using π pulses is to substitute the previous transitions by adiabatic counterparts, such that the method gains stability with respect to changes in the pulse width and intensity at the expense of increasing the area of the pulses. This extension of the parking mechanism, derived in cooperation with I. R. Solá, was successfully applied to the H₂POSH model system [125], as shown in figure 4.17.

Figure 4.17 illustrates the sequence of linearly polarized pulses based on the parking mechanism, with the corresponding evolution of the population dynamics and localization. Since the adiabatic transitions simply replace the π or half- π transitions of the multiple- π pulse scheme, the time-dependent localization in both strategies follows the same dynamic pattern. However, the adiabatic scheme can be considered as a three-step process, as schematically pictured in fig. 4.18.

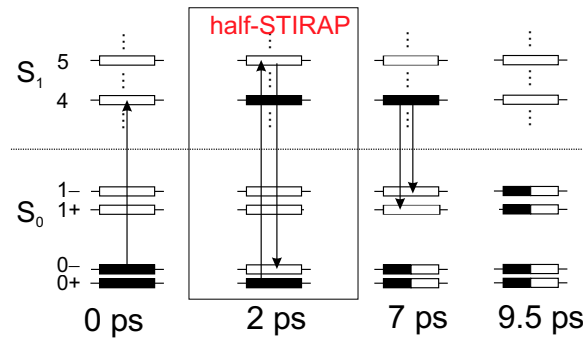


Figure 4.18: Selective transitions of the extended three-step parking mechanism induced by linearly polarized chirped laser pulses and a half-STIRAP passage.

The π -pulse of the first-step (or “parking” step) of the parking mechanism is substituted by a linearly polarized linearly chirped pulse¹³. The parking pulse fully transfers

¹²The global area can be reduced slightly by using simultaneous deexcitation for the fourth and fifth step of the process.

¹³For a linearly chirp pulse the frequency changes with time, it does not have to match exactly the resonance of the transition to ensure full population transfer; instead the frequency sweep should span the resonant frequency. The pulse area of such pulses is limited to a minimum value for the so-called adiabatic passage (for a more detail discussion refer to [135]). However, the pulse area can be increased without damaging the passage.

the population of $|\Phi_{0-}^0\rangle$ to the torsional state $|\Phi_4^1\rangle$ in 2 ps. The sum of the second and third steps together is equivalent to half population transfer in a 3-level Λ system as used for stimulated Raman adiabatic passage (STIRAP) which is in general a paradigm for full population transfer in this type of systems. Therefore, a half-STIRAP process that transfers only 50% of population in a Λ system was developed [125]. The second and third step are substituted by this half-STIRAP process using a Stokes y-polarized pulse preceding the pump z-polarized pulse. The half-STIRAP process drives approximately 50% of the population of $|\Phi_{0+}^0\rangle$ to the other member of the doublet $|\Phi_{0-}^0\rangle$ in 5 ps. The two-photon Raman transition is mediated by the state $|\Phi_5^1\rangle$ and does not interfere with the parking state. This intermediate state is barely populated (less than 4%) during the laser action.

The fourth and fifth steps are implemented together by using two chirped pulses of different polarizations that drive the population from the parking state $|\Phi_4^1\rangle$ to an almost even coherent superposition of $|\Phi_{1+}^0\rangle$ and $|\Phi_{1-}^0\rangle$, which is localized on the left well of S_0 . Since here both transitions compete in the passage, the Rabi frequencies must be exactly equal for obtaining a localized state with 50% population in each member. Besides, since both overlapped subpulses have the same pulse duration, different amplitudes are required to balance the dipole moments, so that both competing transitions have the same Rabi frequency.

The overall adiabatic process implies a global area of approximately 44π to be shared between 5 pulses. This is eleven times larger than the minimum area of the multiple- π strategy discussed before. Since the maximum field amplitude is limited to avoid competing processes in the excitation, the minimum time is fixed by the area requirements. The results presented in fig. 4.17 provide almost the minimum time for adiabatic selection, which is 9.5 ps. Although this time is close to the tunneling rates from the first excited doublet ($\tau_1/2 = 16.8$ ps), since only the last step involves populating this doublet, the localization is not severely spoiled in the adiabatic strategy. Nevertheless, the adiabatic scheme has other advantages, as the larger stability with respect to variations in the amplitude, width and frequency of the pulses. However, perfect localization demands controlling the time duration or the relative amplitude of the pulses. In principle, in molecules with higher internal barriers the tunneling rates should be larger and, therefore, the time limitations are smaller. In those cases the advantages of the adiabatic scheme may become more relevant. Also in the adiabatic strategy one excitation path involves a half-STIRAP process which is used to localize the population in the ground torsional doublet. Since this Raman step involves only little population in the torsional state of the electronic excited potential (it is a dark state) it is less sensitive to the instability of this potential which has just recently been shown to be repulsive along the P-S bond [130], see also section 4.8.

4.6.5 Extensions of the model including coupled overall rotation and internal torsions

In the previous sections the model system was assumed to be pre-oriented, i.e. non-rotating, allowing only the terminal hydrogen to rotate around the P-S bond. This implies that the H_2PO fragment is not influenced by the torsional motion of the terminal hydrogen, i.e. no coupling between the SH and H_2PO fragments exists. This approximation is valid as long as the two fragments differ very much in mass so that the motion of the single hydrogen does not affect the rest of the molecule. Specifically, in the case of the H_2POSH the moment of inertia (with respect to the z-axis) of the H_2PO -fragment ($I_{\text{H}_2\text{PO}} = 1.80\text{amu}$) is 15 times larger than that of the SH-fragment ($I_{\text{SH}} = 30.7\text{amu}$). Still, since a coupling between the SH and the H_2PO -fragment could reduce the enantiomer selectivity of the parking mechanism, free molecular rotations around the P-S bond will be introduced to the model. In this extension the molecule is considered to be in the electronic ground state S_0 without any electronic transitions taken place.

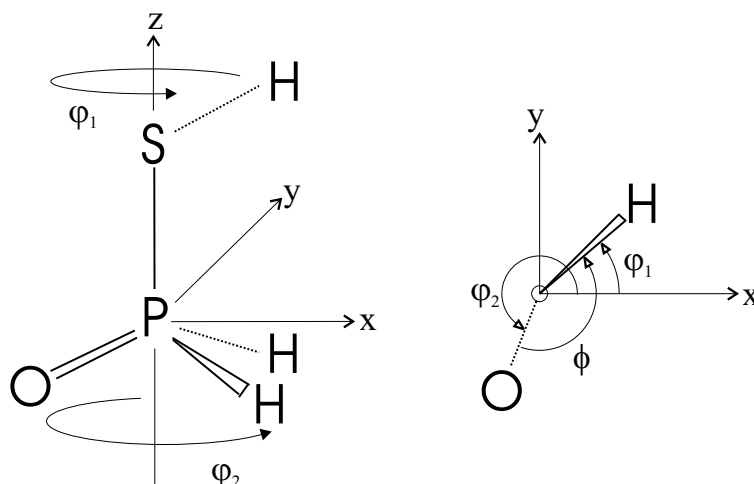


Figure 4.19: The model system, H_2POSH , with the SH and H_2PO fragment carrying out rotational and torsional motions around the oriented P-S bond.

For the extended model system including overall rotation of the molecule, H_2POSH is assumed to be pre-oriented with its torsional axis, i.e. its P-S bond, along the space-fixed z-axis, in accordance with the previous model. Further, the molecule is considered to consist of two fragments, namely SH and H_2PO , as sketched in Figure 4.19, which may rotate around the common axis, the P-S bond. For this two-dimensional model, all degrees of freedom are neglected except the torsional motion of the two fragments relative

to each other where ϕ is the torsional angle, i.e. the OP SH dihedral angle¹⁴. Equivalent negative and positive values of ϕ correspond to opposite configurations of the *L*- and *R*-enantiomers, respectively.

The corresponding moments of inertia with respect to the space-fixed z-axis are for the SH-fragment $I_1 = 1.80 \text{ amu } \text{Å}^2$ and for the H₂PO-fragment $I_2 = 30.7 \text{ amu } \text{Å}^2$. Then, the reduced I_r and the total I_t moments of inertia are defined as

$$\begin{aligned} I_r &= \frac{I_1 I_2}{I_t} \\ I_t &= I_1 + I_2 \end{aligned} \quad (4.20)$$

with $I_r = 1.70 \text{ amu } \text{Å}^2$ and $I_t = 32.5 \text{ amu } \text{Å}^2$ for H₂POSH.

The rotational angle of the SH-fragment around the z-axis is called φ_1 and the rotational angle of the H₂PO-fragment is accordingly denoted by φ_2 , as sketched in Figure 4.19. The torsional angle ϕ and the complementary angle of the overall rotation θ are related to φ_1, φ_2 by

$$\begin{aligned} \phi &= \varphi_1 - \varphi_2 \\ \theta &= \frac{I_1}{I_t} \varphi_1 + \frac{I_2}{I_t} \varphi_2 \end{aligned} \quad (4.21)$$

By definition, the domains of φ_1 and φ_2 are cyclic (modulo 2π), implying also cyclic boundary conditions for ϕ , but in general non-cyclic lower (*l*) and upper (*u*) bounds for θ depending on ϕ (for details see ref. [136]):

$$\begin{aligned} -\pi &\leq \varphi_1 \leq \pi \quad \text{mod } 2\pi \\ -\pi &\leq \varphi_2 \leq \pi \quad \text{mod } 2\pi \\ -\pi &\leq \phi \leq \pi \quad \text{mod } 2\pi \\ l(\phi) &\leq \theta \leq u(\phi) \end{aligned} \quad (4.22)$$

Cyclic boundary conditions for θ

$$-\pi \leq \theta \leq \pi \quad \text{mod } 2\pi \quad (4.23)$$

are obtained only for the special case of equivalent fragments ($I_1 = I_2$), or in the limits where $I_1/I_2 \rightarrow 1$ or $I_2/I_1 \rightarrow 0$ or

$$\frac{I_1}{I_2} \rightarrow 0 \quad (4.24)$$

¹⁴The distance between the fragments, i.e. the P-S bond length (2.115 Å) is kept fixed during the torsional/rotational motion.

implying $\frac{I_1}{I_t} \rightarrow 0$ and, hence, $\theta \rightarrow \varphi_2$. Since for H₂POSH I_1 is much smaller than I_2 , relation (4.24) and, therefore, also relation (4.23), are fulfilled approximately.

For the torsional and rotational motion the molecular model Hamiltonian is set up as:

$$\begin{aligned}
 \hat{\mathbf{H}}_{mol} &= \hat{\mathbf{T}} + \hat{\mathbf{V}} \\
 &= -\frac{\hbar^2}{2I_1} \frac{\partial^2}{\partial \varphi_1^2} - \frac{\hbar^2}{2I_2} \frac{\partial^2}{\partial \varphi_2^2} + V_0(\varphi_1 - \varphi_2) \\
 &= -\frac{\hbar^2}{2I_t} \frac{\partial^2}{\partial \phi^2} - \frac{\hbar^2}{2I_r} \frac{\partial^2}{\partial \theta^2} + V_0(\phi) \\
 &= \hat{\mathbf{H}}_{rot} + \hat{\mathbf{H}}_{tor}.
 \end{aligned} \tag{4.25}$$

These expressions for the molecular Hamiltonian in terms of φ_1 and φ_2 or ϕ and θ are equivalent, but they imply different ways for indicating the couplings of the torsional and rotational motions, either via the potential $V_0(\varphi_1 - \varphi_2)$, or via the boundary condition (4.22) for θ depending on ϕ . For the potential $V_0(\phi) = V_0(\varphi_1 - \varphi_2)$ the one-dimensional *ab initio* PES of the electronic ground state S_0 from ref. [61], calculated at MP2/6-311G(2d,p) level of theory, is used.¹⁵

The molecular eigenfunctions $|\Psi_n\rangle$ of the model Hamiltonian (4.25) are obtained as solutions of the TISE $\hat{\mathbf{H}}_{mol} |\Psi_n\rangle = E_n |\Psi_n\rangle$ subject to the cyclic boundary conditions (4.22):

$$|\Psi_n(\varphi_1, \varphi_2)\rangle = |\Psi_n(\varphi_1 + 2\pi, \varphi_2)\rangle = |\Psi_n(\varphi_1, \varphi_2 + 2\pi)\rangle \tag{4.26}$$

and the normalization

$$\langle \Psi_n | \Psi_n \rangle = 1 \tag{4.27}$$

with scalar product

$$\langle \Psi_m | \Psi_n \rangle = \int_{-\pi}^{\pi} d\varphi_1 \int_{-\pi}^{\pi} d\varphi_2 \Psi_m^*(\varphi_1, \varphi_2) \Psi_n(\varphi_1, \varphi_2). \tag{4.28}$$

Since φ_1 and φ_2 are coupled via the potential $V_0(\varphi_1 - \varphi_2)$, no simple analytic solution for the TISE can be derived. In general, the solution has to be obtained numerically (for details see ref. [136]). However, a simple approximate solution valid for H₂POSH, because $I_1 \ll I_2$, i.e. close to the limit (4.24) implying the approximate boundary condition (4.23), exists. This approximate solution (indicated by a tilde) is obtained by solving the TISE in terms of the coordinates ϕ and θ ,

$$\begin{aligned}
 \left[\hat{\mathbf{H}}_{rot} + \hat{\mathbf{H}}_{tor} \right] \left| \tilde{\Psi}_n(\phi, \theta) \right\rangle &= \left[-\frac{\hbar^2}{2I_r} \frac{\partial^2}{\partial \phi^2} - \frac{\hbar^2}{2I_t} \frac{\partial^2}{\partial \theta^2} + V_0(\phi) \right] \left| \tilde{\Psi}_n(\phi, \theta) \right\rangle \\
 &= E_n \left| \tilde{\Psi}_n(\phi, \theta) \right\rangle,
 \end{aligned} \tag{4.29}$$

¹⁵This potential differs only slightly from the previously discussed PES of the one-dimensional model shown in fig. 4.5.

with rigorous and approximate boundary conditions for ϕ and θ , respectively,

$$\left| \tilde{\Psi}_n(\phi, \theta) \right\rangle = \left| \tilde{\Psi}_n(\phi + 2\pi, \theta) \right\rangle \approx \left| \tilde{\Psi}_n(\phi, \theta + 2\pi) \right\rangle \quad (4.30)$$

and corresponding approximate normalizations

$$\left\langle \tilde{\Psi}_n \left| \tilde{\Psi}_n \right\rangle \approx \int_{-\pi}^{\pi} d\phi \int_{-\pi}^{\pi} d\theta \tilde{\Psi}_n^*(\phi, \theta) \tilde{\Psi}_n(\phi, \theta) = 1 \quad (4.31)$$

Equations (4.29)-(4.31) imply the approximate separation of the torsional (ϕ) and overall rotational (θ) motions. Thus, the corresponding eigenfunctions are written as products

$$\left| \tilde{\Psi}_{v\pm, M}(\phi, \theta) \right\rangle := \left| \tilde{\Psi}_n(\phi, \theta) \right\rangle = |\Phi_{v\pm}(\phi)\rangle \cdot |\Theta_M(\theta)\rangle. \quad (4.32)$$

The torsional eigenfunctions $|\Phi_{v\pm}(\phi)\rangle$ in eqn. (4.32) are, in accordance with the previously used 1D-model, solutions of the torsional Schrödinger equation

$$\hat{\mathbf{H}}_{tor} |\Phi_{v\pm}\rangle = \left[-\frac{\hbar^2}{2I_r} \frac{\partial^2}{\partial \phi^2} + V_0(\phi) \right] |\Phi_{v\pm}(\phi)\rangle = E_{v\pm} |\Phi_{v\pm}(\phi)\rangle \quad (4.33)$$

with eigenenergies $E_{v\pm}$, illustrated in figure 4.5¹⁶ and the torsional quantum numbers $v\pm = 0+, 0-, 1+, 1-, 2+, 2-, \dots$ with + and - for symmetric and anti-symmetric eigenfunctions with respects to inversion at $\phi = 0^\circ$.

Likewise, the approximate overall rotational wave functions $|\Theta_M(\theta)\rangle$ satisfy the rotational Schrödinger equation

$$\hat{\mathbf{H}}_{rot} |\Theta_M(\theta)\rangle = -\frac{\hbar^2}{2I_t} \frac{\partial^2}{\partial \theta^2} |\Theta_M(\theta)\rangle = E_M |\Theta_M(\theta)\rangle, \quad (4.34)$$

implying the analytical solutions for the eigenenergies

$$E_M = \frac{\hbar^2 M^2}{2I_t} \quad (4.35)$$

and the eigenfunctions

$$|\Theta_M(\theta)\rangle = \frac{1}{\sqrt{2\pi}} e^{iM\theta}, \quad (4.36)$$

with $M = \dots - 2, -1, 0, 1, 2, \dots$. For $M \neq 0$, the eigenstates are degenerate.

¹⁶The eigenenergies shown in fig. 4.5 are based on I_1 instead of the reduced moment of inertia I_r used for the 2D model.

The resulting products of torsional eigenfunctions $|\Phi_{v\pm}(\phi)\rangle$ and rotational eigenfunctions $|\Theta_M(\theta)\rangle$

$$\begin{aligned} |\tilde{\Psi}_{v\pm,M}(\phi, \theta)\rangle &= |\Phi_{v\pm}(\phi)\rangle \cdot |\Theta_M(\theta)\rangle, \\ v = 0, 1, 2, \dots, \quad M &= \dots - 2, -1, 0, 1, 2, \dots \end{aligned} \quad (4.37)$$

are exact ($M = 0$) or approximate ($M \neq 0$) eigenfunctions of $\hat{\mathbf{H}}_{mol}$ with eigenvalues

$$\tilde{E}_{v\pm,M} = E_{v\pm} + \frac{\hbar^2 M^2}{2I_t}. \quad (4.38)$$

For the present model system where $I_1/I_2 \ll 1$, the approximate complex eigenfunctions $|\tilde{\Psi}_{v\pm,M}\rangle$ and eigenenergies $\tilde{E}_{v\pm,M}$, which satisfy the TISE together with the approximate boundary conditions (4.30) and normalization (4.31), should be similar to the corresponding exact solutions of the TISE, which satisfy the rigorous boundary condition (4.26) and normalization (4.27):

$$|\Psi_n\rangle = |\Psi_{v\pm,M}\rangle \approx |\tilde{\Psi}_{v\pm,M}\rangle, \quad (4.39)$$

$$E_n = E_{v\pm,M} \approx \tilde{E}_{v\pm,M}, \quad (4.40)$$

with $n = 0, 1, 2, \dots$, $v = 0, 1, 2, \dots$ and $M = \dots, -2, -1, 0, 1, 2, \dots$. For $M = 0$, the approximations (4.39) and (4.40) become exact due to the absence of rotational/torsional coupling. These approximations, involved in expressions (4.39) and (4.40) are a consequence of the approximate validity of the cyclic boundary condition (4.23), due to the very small ratio of the moments of inertia $I_1/I_2 \ll 1$ for the present system; this implies that the $|\Psi_{v\pm,M}\rangle$'s should have "good" torsional and rotational quantum numbers v and M , respectively. Hence, in analogy to the localized torsional functions $|\Phi_{vR}\rangle$, $|\Phi_{vL}\rangle$, from the exact complex $|\Psi_{v+,M}\rangle$ and $|\Psi_{v-,M}\rangle$ localized wave functions $|\Psi_{vL,M}\rangle$ and $|\Psi_{vR,M}\rangle$ ($M = -2, -1, 0, 1, 2, \dots$) can be constructed for the L - and R -enantiomers, respectively:

$$\begin{aligned} |\Psi_{vL,M}\rangle &= \frac{1}{\sqrt{2}} (|\Psi_{v+,M}\rangle + |\Psi_{v-,M}\rangle) \\ |\Psi_{vR,M}\rangle &= \frac{1}{\sqrt{2}} (|\Psi_{v+,M}\rangle - |\Psi_{v-,M}\rangle) \end{aligned} \quad (4.41)$$

In practice, the wave functions $|\Psi_{v\pm,M}\rangle$ and energies $E_{v\pm,M}$ were calculated by diagonalizing the molecular Hamiltonian $\hat{\mathbf{H}}_{mol}$ by means of basis functions which satisfy the rigorous boundary conditions (4.26) and normalizations (4.27). In figure 4.20 the resulting torsional/rotational eigenenergies as well as their approximated values derived from

(4.38) are shown. As expected, exact and approximate values differ very little and show no significant effect on the dynamical simulations.

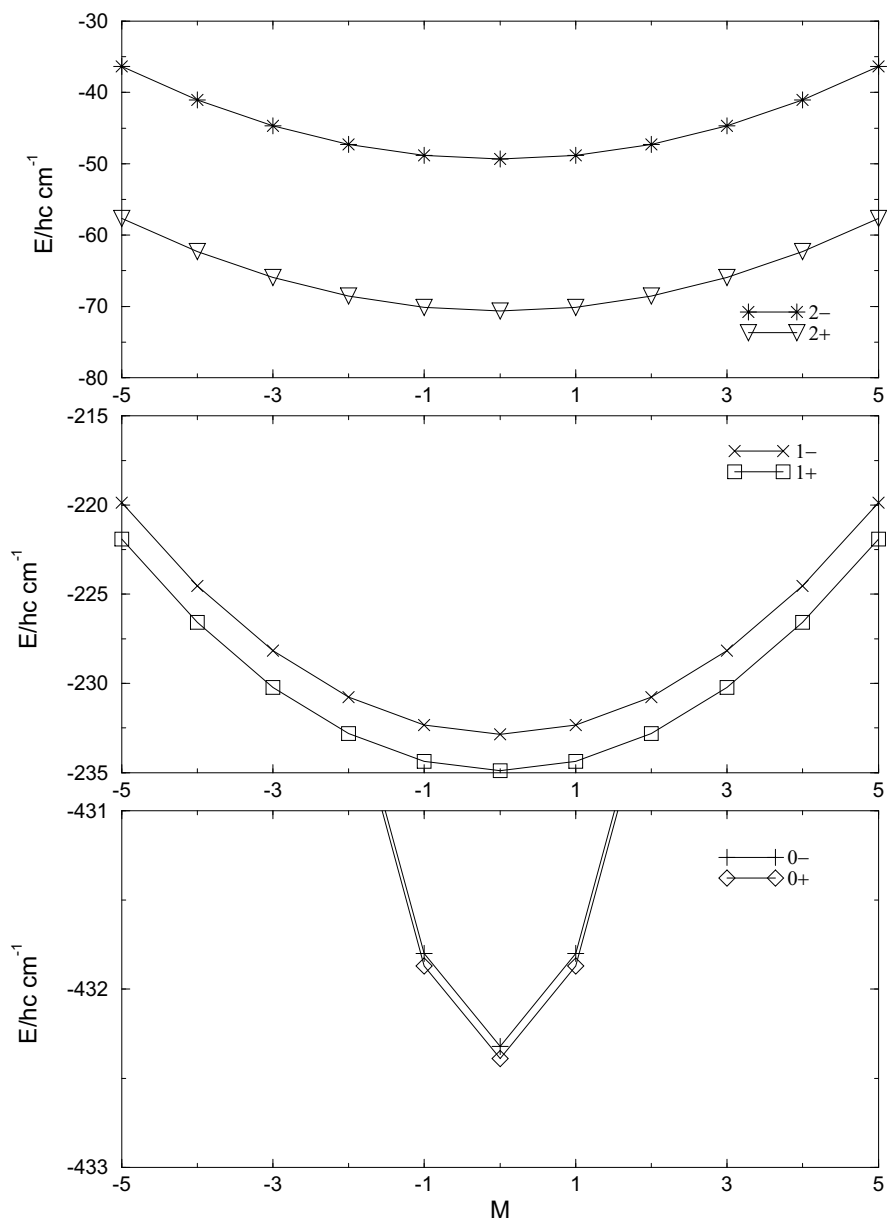


Figure 4.20: Accurate (symbols) and approximate (continuous lines) values of the torsional ($v+$ or $v-$) and rotational (M) energies $E_{v\pm,M}$ of the model H₂POSH. Note the different scales for $v = 0, 1$ and 2 . (adapted from ref. [136])

For the wave packet propagation the TDSE has to be solved numerically. The propagation starts from a racemate:

$$\begin{aligned}
 \rho_{rac}(T \rightarrow 0) &= |\Psi_{0+,0}\rangle \frac{1}{2} \langle \Psi_{0+,0}| + |\Psi_{0-,0}\rangle \frac{1}{2} \langle \Psi_{0-,0}| \\
 &= |\Psi_{0L,0}\rangle \frac{1}{2} \langle \Psi_{0L,0}| + |\Psi_{0R,0}\rangle \frac{1}{2} \langle \Psi_{0R,0}| \\
 &= \rho_{0L,0}(T) + \rho_{0R,0}(T).
 \end{aligned} \tag{4.42}$$

Here it is important to note that the initial temperature T of the system has to be much lower than in the 1D model to fulfill the initial condition (4.42), because the rotational excitation from $M = 0$ to $M = \pm 1$ costs less than 1 cm^{-1} (see figure 4.20).

The time dependent populations are given, in analogy to the 1D-model, by

$$P_{v\pm,M}(t) = |\langle \Psi_{v\pm,M} | \Psi_{0\pm,0}(t) \rangle|^2, \tag{4.43}$$

with $|\Psi_{0\pm,0}(t)\rangle$ being the time-dependent wave function in the electronic ground state potential S_0 . Likewise, the populations of the states representing the L - or R -enantiomers are obtained

$$P_{vL/R,M} = |\langle \Psi_{vL/R,M} | \Psi_{0\pm,0}(t) \rangle|^2. \tag{4.44}$$

The overall populations of the L - or R -enantiomers are obtained by summing up all the populations of the torsional/rotational states of the left or right enantiomers, respectively,

$$P_{L/R} = \sum_v \sum_M P_{vL/R,M} \tag{4.45}$$

The laser driven wave packet dynamics are simulated by means of the TDSE using the Hamiltonian $\hat{\mathbf{H}}(t) = \hat{\mathbf{H}}_{mol} - \vec{E}_{\pm}(t) \cdot \vec{\mu}$ in the semi-classical dipole approximation. For molecular control circularly polarized laser pulses are employed instead of linearly polarized fields, as used for the 1D model. The circularly right (+) or left (−) polarized laser pulses $\vec{E}_{i\pm}(t)$ propagate along the z -axis and are given by

$$\vec{E}_{i\pm}(t) = E_i^0 \cdot \sin^2\left(\frac{\pi(t - t_{d_i})}{t_{p_i}}\right) \cdot (\cos[\omega_i(t - t_{d_i}) + \eta_i], \pm \sin[\omega_i(t - t_{d_i}) + \eta_i], 0)^T. \tag{4.46}$$

The components of the dipole moment $\vec{\mu}$ in the laboratory fixed frame (x, y) can be

expressed in terms of molecular fragment fixed coordinates (x_1, y_1) or (x_2, y_2) :

$$\vec{\mu} = \begin{pmatrix} \mu_x(\varphi_1, \varphi_2) \\ \mu_y(\varphi_1, \varphi_2) \end{pmatrix} \quad (4.47)$$

$$= \begin{pmatrix} \cos \varphi_2 & -\sin \varphi_2 \\ \sin \varphi_2 & \cos \varphi_2 \end{pmatrix} \begin{pmatrix} \mu_{x_2}(\varphi_1 - \varphi_2) \\ \mu_{y_2}(\varphi_1 - \varphi_2) \end{pmatrix} \quad (4.48)$$

$$= \begin{pmatrix} \cos \varphi_1 & -\sin \varphi_1 \\ \sin \varphi_1 & \cos \varphi_1 \end{pmatrix} \begin{pmatrix} \mu_{x_1}(\varphi_2 - \varphi_1) \\ \mu_{y_1}(\varphi_2 - \varphi_1) \end{pmatrix} \quad (4.49)$$

$$\approx \begin{pmatrix} \mu_x(\phi, \theta) \\ \mu_y(\phi, \theta) \end{pmatrix}, \quad (4.50)$$

where the subindices 1 and 2 label the SH-fragment and the H₂PO-fragment, respectively. The two transformations from the laboratory fixed to the molecular fragment fixed components of the dipole moment $\vec{\mu}$ are equivalent since

$$\begin{pmatrix} \mu_{x_1}(\varphi_2 - \varphi_1) \\ \mu_{y_1}(\varphi_2 - \varphi_1) \end{pmatrix} = \begin{pmatrix} \cos(\varphi_2 - \varphi_1) & -\sin(\varphi_2 - \varphi_1) \\ \sin(\varphi_2 - \varphi_1) & \cos(\varphi_2 - \varphi_1) \end{pmatrix} \begin{pmatrix} \mu_{x_2}(\varphi_1 - \varphi_2) \\ \mu_{y_2}(\varphi_1 - \varphi_2) \end{pmatrix}. \quad (4.51)$$

In practice, the expression in terms of the coordinates of the heavier fragment, i.e. the components μ_{x_2} and μ_{y_2} , is used. The induced transitions from torsional/rotational states $|\Psi_{v'\pm, M'}\rangle$ to $|\Psi_{v\pm, M}\rangle$ are evaluated in terms of the dipole transition matrix elements. Two contributions, one for absorption (*ab*) and one for emission (*em*) processes are distinguished:

$$\begin{aligned} \langle \Psi_{v\pm, M} | \vec{E}_{i\pm} \cdot \vec{\mu} | \Psi_{v'\pm, M'} \rangle &= \langle \Psi_{v\pm, M} | \vec{E}_{i\pm}^{ab} \cdot \vec{\mu} | \Psi_{v'\pm, M'} \rangle + \langle \Psi_{v\pm, M} | \vec{E}_{i\pm}^{em} \cdot \vec{\mu} | \Psi_{v'\pm, M'} \rangle \\ &\equiv -\frac{1}{2} E_i^0 \cdot \sin^2 \left(\frac{\pi(t - t_{d_i})}{t_{p_i}} \right) \\ &\times \{ e^{i[\omega_i(t-t_{d_i})+\eta_i]} \langle \Psi_{v\pm, M} | \hat{\mu}_{\pm} | \Psi_{v'\pm, M'} \rangle \\ &+ e^{-i[\omega_i(t-t_{d_i})+\eta_i]} \langle \Psi_{v\pm, M} | \hat{\mu}_{\mp} | \Psi_{v'\pm, M'} \rangle \} \end{aligned} \quad (4.52)$$

where the dipole operators $\hat{\mu}_{\pm}$ are given in laboratory-fixed coordinates, $\hat{\mu}_{\pm} = \mu_x(\varphi_1, \varphi_2) \pm i\mu_y(\varphi_1, \varphi_2) = e^{\pm i\varphi_2} (\mu_{x_2}(\varphi_1 - \varphi_2) \pm i\mu_{y_2}(\varphi_1 - \varphi_2))$. The $\hat{\mu}_{\pm} | \Psi_{v\pm, M} \rangle$ are eigenstates of the angular momentum operator $\hat{\mathbf{L}}_z = -i\hbar \frac{\partial}{\partial \theta}$ along the z-axis, with eigenvalues $(M \pm 1)\hbar$:

$$\hat{\mathbf{L}}_z \hat{\mu}_{\pm} | \Psi_{v\pm, M} \rangle = \hbar(M \pm 1) \hat{\mu}_{\pm} | \Psi_{v\pm, M} \rangle. \quad (4.53)$$

The dipole matrix elements $\langle \Psi_{v\pm, M} | \hat{\mu}_{\pm} | \Psi_{v'\pm, M'} \rangle$ in eqn. (4.52) vanish unless $M = M' \pm 1$

(for details see [136])¹⁷. This implies the rotational selection rules

$$\begin{aligned} M &= M' \pm 1 \text{ for absorption with left/right polarized light} \\ M &= M' \mp 1 \text{ for emission with left/right polarized light} \end{aligned} \quad (4.55)$$

i.e. right polarized light induces absorption and emission processes which decrease or increase the rotational quantum numbers M by -1 or $+1$, respectively, and vice versa for left polarized light.

For the transitions between states with different torsional quantum numbers the same selection rules apply as for the 1D-model, i.e. transitions between states v and v' with the same symmetries $+$ or $-$, are mediated by μ_{x_2} ($\hat{=} \mu_x^{00}$ in fig. 4.6), whereas transitions between states with opposite symmetries $+$, $-$ are mediated by μ_{y_2} ($\hat{=} \mu_y^{00}$ in fig. 4.6).

Based on the experience with the laser control of the simpler non-rotating model system a new “parking” mechanism was designed with extensions for the overall rotation of the molecule. In practice, this extended mechanism was developed by making a “learned guess” for a series of laser pulses similar to that of the non-rotating model [128], but taking into account the selection rules (4.55) for the rotational transitions in the present torsional/rotational model. Together with a suitable choice of individual laser-dipole transition elements for the transitions involved, the laser parameters were optimized for each of the individual transitions, until the optimal series of laser pulses for the overall series of transitions were obtained¹⁸.

The resulting series of four circular polarized pulses which drives the initial density, representing a model racemate of oriented H₂POSH molecules at low temperature, to a (nearly) pure R -enantiomer, is illustrated in Figure 4.21. Also shown are the corresponding population dynamics of the dominant levels $|\Psi_{v\pm, M}\rangle$ as well as the populations P_R and P_L , which specify the localizations of the wave packet. The corresponding parameters, the polarizations, and the dominant transitions induced by the pulses, are listed in table 4.5.

¹⁷In case of the approximate solution one obtains e.g.:

$$\begin{aligned} &\langle \tilde{\Psi}_{v\pm, M}(\phi, \theta) | \hat{\mu}_{\pm}(\phi, \theta) | \tilde{\Psi}_{v'\pm, M'}(\phi, \theta) \rangle \\ &= \langle \Theta_M(\theta) | e^{\pm i\theta} | \Theta_{M'}(\theta) \rangle \langle \Phi_{v\pm}(\phi) | \mu_{x_2}(\phi) \pm i\mu_{y_2}(\phi) | \Phi_{v'\pm} \rangle, \end{aligned} \quad (4.54)$$

where $\langle \Theta_M | e^{\pm i\theta} | \Theta_{M'} \rangle = \delta_{M, M' \pm 1}$.

¹⁸Some subpulses were first obtained from the local control method (see section 2.4.3) and afterwards optimized by hand.

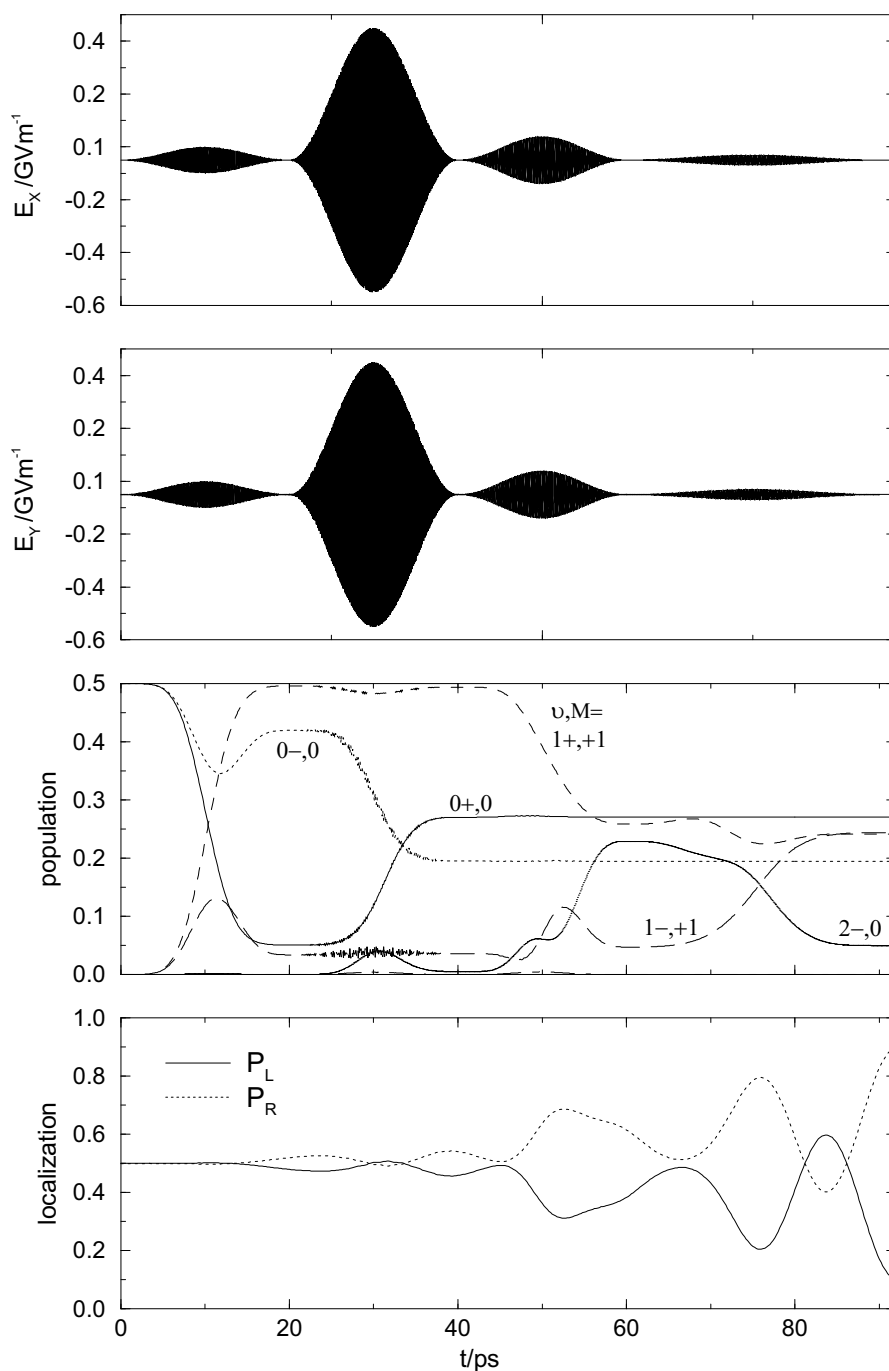


Figure 4.21: Top panel: Electrical field amplitudes E_x and E_y of the circular polarized laser pulses. Middle panel: Resulting populations of the dominant torsional/rotational levels (quantum numbers are given as $v\pm, M$). Bottom panel: Localizations, i.e. total populations P_L and P_R of the L - and R -enantiomers. (adapted from ref. [136])

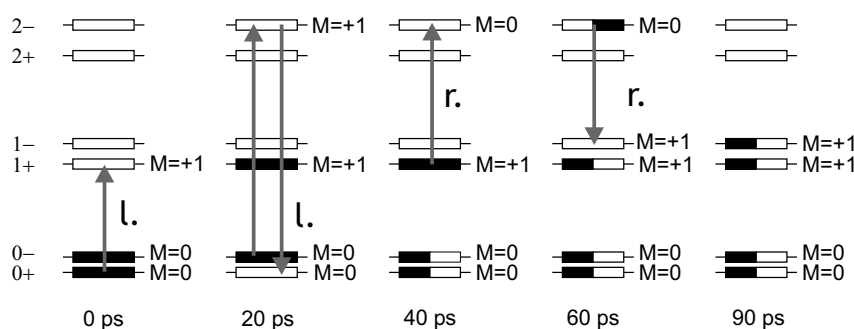


Figure 4.22: Dominant transitions between torsional/rotational eigenstates of H₂POSH as induced by the laser pulse sequence shown in Figure 4.21. The letters $l.$ and $r.$ stand for left and right circularly polarized laser pulses. (adapted from ref. [136])

The resulting dominant populations of states $|\Psi_{v\pm,M}\rangle$ before and after the individual pulses are also indicated schematically in Figure 4.22. Accordingly, the first laser pulse ($i = 1$) transfers most of the population of $|\Psi_{0+,0}\rangle$ into $|\Psi_{1+,+1}\rangle$. This population is kept nearly constant during the second laser pulse ($i = 2$) – it is “parked” in level $|\Psi_{1+,+1}\rangle$. The second pulse transfers approximately one half of the population of the states $|\Psi_{0-,0}\rangle$ via $|\Psi_{2-,+1}\rangle$ into $|\Psi_{0+,0}\rangle$. The intermediate populations of $|\Psi_{2-,+1}\rangle$ are rather small, nevertheless the transition via $|\Psi_{2-,+1}\rangle$ is implied by the carrier frequency, polarization, and the duration of the second laser pulse. The net effect of the second laser pulses is therefore ca. 50% transfer from $|\Psi_{0-,0}\rangle$ back to $|\Psi_{0+,0}\rangle$, thus creating a coherent superposition of the levels $|\Psi_{0+,0}\rangle$ and $|\Psi_{0-,0}\rangle$ which is different from the initial incoherent preparation of the racemate in the same states. The new coherence arises from the manipulation of one of the initial eigenstates, i.e. $|\Psi_{0-,0}\rangle$, by means of coherent laser pulses. On the other hand, the initial incoherence in the two initial eigenstates, $|\Psi_{0+,0}\rangle$ and $|\Psi_{0-,0}\rangle$ or, alternatively, $|\Psi_{0R,0}\rangle$ and $|\Psi_{0L,0}\rangle$ is not lost – it has been transferred into incoherent populations of the “parking” state $|\Psi_{1+,+1}\rangle$ and of the coherent lowest ($v = 0, M = 0$) doublet of states, $|\Psi_{0+,0}\rangle$ and $|\Psi_{0-,0}\rangle$. The third ($i = 3$) and fourth ($i = 4$) laser pulses leave that coherent torsional/rotational ground state doublet of states nearly unaffected, allowing its coherent tunneling (see fig. 4.21) until most of its population is localized in the ground state of the R -enantiomer, $|\Psi_{0R,0}\rangle$. Simultaneously, the third pulse transfers ca. 50% of the population of the “parking” state $|\Psi_{1+,+1}\rangle$ into $|\Psi_{2-,0}\rangle$, whereas the fourth pulse transfers that population from $|\Psi_{2-,0}\rangle$ into $|\Psi_{1-,+1}\rangle$, thus creating a coherent superposition in the first torsionally ($v = 1$) and rotationally ($M = +1$) excited doublet of states, $|\Psi_{1+,+1}\rangle$ and $|\Psi_{1-,+1}\rangle$. The net effect of the third and fourth laser pulses is thus: population transfer from the “parking” state $|\Psi_{1+,+1}\rangle$ into a coherent superposition of the doublet of states, $|\Psi_{1+,+1}\rangle$ and $|\Psi_{1-,+1}\rangle$, while leaving the ground state doublet of states unaffected. As anticipated in section 2.4.1, the field strengths of the individual laser pulses correspond

Table 4.5: Parameters of the series of laser pulses, preparing the *R*-enantiomer of H₂POSH from a racemate.

pulse number <i>i</i>	field amplitude $E_i/(V/m)$	pulse duration t_i/ps	delay time t_{p_i}/ps	carrier frequency $\omega_i/hc \text{ cm}^{-1}$	pulse phase η_i	polarization (l/r)	dominant rot./tor. trans. $v\pm, M \xrightarrow{ab,em} v'\pm, M'$
1	$5 \cdot 10^7$	20	0	198.00	$-\pi/2$	l	$0+, 0 \xrightarrow{ab} 1+, +1$
2	$5 \cdot 10^8$	20	20	383.57	$-\pi/2$	l	$0-, 0 \xrightarrow{ab} (2-, +1)$ $\xrightarrow{em} 0+, 0$
3	$9 \cdot 10^7$	20	40	185.03	0	r	$1+, +1 \xrightarrow{ab} 2-, 0$
4	$2 \cdot 10^7$	30	60	182.99	0	r	$2-, 0 \xrightarrow{em} 1-, +1$

roughly to π -pulses.

The coherences in the doublets $v = 0$ and $v = 1$ allow tunneling which, ultimately, yield simultaneous localizations in the two torsional/rotational ground and excited states, $|\Psi_{0R,0}\rangle$ as well as $|\Psi_{1R,+1}\rangle$. The sum of these populations at the end of the series of laser pulses is the overall, close to 90% population of the right enantiomer. The origin for the ca. 10% missing population in the target R -enantiomer, is the result of mainly the first laser pulse. Close inspection of Fig. 4.21 indicates that this pulse does not only transfer population from $|\Psi_{0+,0}\rangle$ into $|\Psi_{1+,+1}\rangle$, but to some significant (ca. 10%) extent also from $|\Psi_{0-,0}\rangle$ into (mainly) $|\Psi_{1-,+1}\rangle$ but also into $|\Psi_{1+,+1}\rangle$. These simultaneous transfers of populations, not only from $|\Psi_{0+,0}\rangle$ but also from $|\Psi_{0-,0}\rangle$, are a consequence of the near degeneracy of the initial and final states which are depopulated or populated during the first laser pulse. The more efficient transfer from $|\Psi_{0+,0}\rangle$ to $|\Psi_{1+,+1}\rangle$, in comparison with the transfers from $|\Psi_{0-,0}\rangle$ to $|\Psi_{1-,+1}\rangle$ or $|\Psi_{1+,+1}\rangle$, is, indeed, a consequence of the corresponding different dipole transition matrix elements.

As anticipated, the rotational selection rules (4.55) are satisfied during the various absorption (pulses $i = 1, 2, 3$) and stimulated emission ($i = 2, 4$) processes by means of left ($i = 1, 2$) and right ($i = 3, 4$) circular polarized laser pulses. If all the right circular polarizations are changed into left polarizations, and *vice versa*, then the left enantiomer is prepared instead of the right one.

In conclusion, this extended model system allowing overall molecular rotation proved that the enantio-selectivity is somewhat reduced, i.e. to only 90% instead of $\sim 100\%$, and requires circularly polarized laser pulses instead of linearly polarized pulses. From the experimental point of view, this might imply some restrictions to the available frequency domains of current circularly polarized lasers. However, the parking mechanism is a very general control scheme to purify a racemate of a pre-oriented non-rotating or rotating molecules with axial chirality. In the following sections, an even simpler control mechanism will be introduced.

4.7 The enantio-selective pump-dump mechanism

4.7.1 Derivation of a simplified control scheme

The parking mechanism has proven to be efficient to prepare pure enantiomers from a racemic mixture of pre-oriented non-rotating and even rotating H₂POSH atropisomers.

Different modifications of this control scheme, as adiabatic passages or circularly polarized pulses for rotating molecules, have been successfully applied in the previous sections. Still, further simplifications of the mechanism are possible. In the following, another control scheme, the so-called enantio-selective pump-dump mechanism, is derived based on the knowledge gained from the parking mechanism. Note that the enantio-selective pump-dump mechanism has been suggested independently, without the present derivation from the parking mechanism, by Fujimura and Hoki [137].

The parking mechanism can be simplified in several ways. In the previous sections the pump-dump sequence of steps 2 and 3 (section 4.6.4 and 4.6.5) as well as the dump-dump subpulses 4 and 5 (section 4.6.4) were replaced by single laser pulses. In both cases the single pulse can be constructed, in a sense, by overlapping the two subsequent subpulses. In order to retain the enantio-selectivity of the two subpulses, the respective single pulse must be polarized in a specific way. In order to get an idea how the polarization of these pulses has to be chosen in case of the non-rotating model system, it is helpful to take a close look at the relative phases of the subpulses of the parking mechanism.

The relative phase η between the second and third ($\eta = \eta_3 - \eta_2$) as well as between the fourth and the fifth ($\eta = \eta_5 - \eta_4$) linearly polarized subpulses of the original parking sequence (see fig. 4.14) defines the localization of the prepared wave packet in the lowest and first excited doublet of torsional eigenstates, respectively. This relative phase has to be chosen such that the prepared wave packet is preferably localized completely left or right of the central potential barrier *at the end* of the pulse sequence. If for instance, the relative phase between the two respective subpulse is changed by $\pm\pi$, then, the respective opposite localized wave packet will be created. The selectivity of these enantio-selective subpulses is, therefore, controlled by their relative phases. However, the choice of the relative phase is also based on the tunneling times of the respective doublet of eigenstates [129]. After the second subpulse, the prepared wave packet starts to tunnel back and forth through the central barrier of the system. Thus, the end of the second pulse 'defines' the localization of the wave packet and, therefore, η has to be chosen accordingly to accomplish high selectivity.

Because of the selection rules the two subpulses causing enantio-selective transitions have different polarizations. In the case of the fourth and the fifth subpulses which induce transitions to the torsional eigenstates $|\Phi_{1+}\rangle$ and $|\Phi_{1-}\rangle$, the subpulses could easily be overlapped, adjusting their amplitudes, as discussed in section 4.6.2. Then, the two transitions creating a localized wave packet are induced simultaneously and since only during the pulse duration of this single pulse the wave packet can tunnel through the barrier, the relative phase η has to be re-optimized for L/R -selectivity. For $\eta \neq 0$ or $\eta \neq \pm\pi$ the superposition of the two subpulses of different polarization will cause a circularly polarized pulse, as used in section 4.6.5 and in refs. [127, 129, 138] to create

localized wave packets starting from a pure eigenstate of the system. If η is set zero or a multiple of π then a single linearly polarized laser pulse is obtained. The electric field vector $\vec{E}(t)$ of the pulse will be polarized in the plane perpendicular to its direction of propagation; the direction of this vector depends on the amplitudes of its two components or on its polarization angle α . The amplitude of the components are adjusted to the transition dipole matrix elements of the desired transitions for a given pulse duration (see section 2.94). Such a linearly polarized laser pulse can also create a localized wave packet from a pure eigenstate. Therefore, the fourth and five laser pulse of the parking mechanism could be replaced by such an enantio-selective linearly polarized pulse (decreasing the number of pulses from five to four).

If a linearly polarized laser pulse can selectively create a localized wave packet from a pure eigenstate then also the opposite should be possible, i.e. the enantio-selective transfer of the population of a localized wave function to a pure eigenstate. This would allow to further simplify the laser control: The population of the undesired enantiomer is directly transferred to a pure eigenstate and, from there a localized wave packet is selectively created in the desired well of the potential. Before such an enantio-selective conversion of one enantiomer into the other and its implementation for the preparation of pure enantiomers is further discussed, the dependence of the polarization angle α of a linearly polarized laser pulse on the localization of the wave packet prepared from a pure eigenstate is derived.

The enantio-selectivity of a linearly polarized pulse is controlled by the direction of the polarization vector of the laser which is determined such that there is the largest interaction between the laser and the L - or R -enantiomer, while the interaction with the respective opposite form vanishes [137]. Specifically, the direction of the electric field vector \vec{E}^0 has to be chosen such that \vec{E}^0 multiplied by the transition dipole matrix elements between the pure state $|\Phi_{w\pm}\rangle$ and the desired localized state $|\Psi_{vL}\rangle$ or $|\Psi_{vR}\rangle$ becomes zero for the undesired localized state and not zero for the target state:

$$\langle \Phi_{w\pm} | \vec{\mu} | \Psi_{vR} \rangle \cdot \vec{E}^0 = 0 \quad \text{and} \quad (4.56)$$

$$\langle \Phi_{w\pm} | \vec{\mu} | \Psi_{vL} \rangle \cdot \vec{E}^0 \neq 0 \quad \text{with } v = 0, 1, 2, \dots \text{ and } v \neq w, \quad (4.57)$$

in case $|\Psi_{vL}\rangle$ is the desired target state. Since these conditions depend, via the dipole moment $\vec{\mu}$, on the orientation of the molecule, they only hold if L - and R -enantiomers are pre-oriented from the beginning such that they are exact mirror images of each other at the moment of the interaction with the laser pulse. This is implied by the initial conditions of the here used model system starting from a pre-oriented racemic mixture $\frac{1}{2}\rho_{0L} + \frac{1}{2}\rho_{0R}$ in the limit of low temperature.

If the laser field is propagating along the z -axis its polarization vector will be in the

x-y-plane and eqn. (4.56) becomes

$$\begin{aligned} E_x^0 \cdot \langle \Phi_{w\pm} | \mu_x | \Psi_{vR} \rangle + E_y^0 \cdot \langle \Phi_{w\pm} | \mu_y | \Psi_{vR} \rangle &= 0 \quad \Rightarrow \\ E_x^0 \langle \Phi_{w\pm} | \mu_x \frac{1}{\sqrt{2}} (|\Phi_{v+}\rangle - |\Phi_{v-}\rangle) &= -E_y^0 \langle \Phi_{w\pm} | \mu_y \frac{1}{\sqrt{2}} (|\Phi_{v+}\rangle - |\Phi_{v-}\rangle) \end{aligned} \quad (4.58)$$

using the definition for the localized state $|\Psi_{vR}\rangle$. To fulfill the conditions (4.56) and (4.57) the components of the dipole moment (μ_x and μ_y) have to be of different symmetry with respect to inversion at $\phi = 0^\circ$. If μ_x has + symmetry ($\mu_x = \mu_+$) and μ_y has – symmetry ($\mu_y = \mu_-$), then expression (4.58) simplifies based on the selection rules (4.19) to:

$$\pm \frac{1}{\sqrt{2}} \cdot E_+^0 \cdot \langle \Phi_{w\pm} | \mu_+ | \Phi_{v\pm} \rangle = \pm \frac{1}{\sqrt{2}} \cdot E_-^0 \cdot \langle \Phi_{w\pm} | \mu_- | \Phi_{v\mp} \rangle, \quad (4.59)$$

where E_+^0 is the laser field component that couples with μ_+ and E_-^0 the one that couples with μ_- . If, for example, $|\Phi_{w+}\rangle$ is the initial pure state, then based on the selection rules E_+^0 connects it via μ_+ with the $|\Phi_{v+}\rangle$ component of the localized state $|\Psi_{vR}\rangle$ and E_-^0 connects the same pure state via μ_- with the other component of the localized state $|\Phi_{v-}\rangle$.

In analogy of eqn. (4.59) condition (4.57) for the desired target state $|\Psi_{vL}\rangle$ is rewritten by changing the sign of the superposition of eigenstates in (4.58) according to the definition of $|\Psi_{vL}\rangle$:

$$\frac{1}{\sqrt{2}} \cdot E_+^0 \cdot \langle \Phi_{w\pm} | \mu_+ | \Phi_{v\pm} \rangle + \frac{1}{\sqrt{2}} \cdot E_-^0 \cdot \langle \Phi_{w\pm} | \mu_- | \Phi_{v\mp} \rangle = \frac{\hbar\Omega(t)}{s(t)} \neq 0, \quad (4.60)$$

with $\Omega(t)$ being the Rabi frequency and $s(t)$ the envelope function of the laser pulse. The enantio-selective transition based on condition (4.60) is designed essentially as a π pulse for 100% population transfer from the pure state $|\Phi_{w\pm}\rangle$ to the desired localized state, here $|\Psi_{vL}\rangle$, or *vice versa*. For this purpose, the transition frequency is approximated as the energy difference between the pure state $|\Phi_{w\pm}\rangle$ and the energy of the localized state $|\Psi_{vL}\rangle$ ¹⁹:

$$\hbar\omega = E_{w\pm} - \tilde{E}_{vL}, \quad (4.61)$$

where $E_{w\pm}$ denotes the energy of the pure state which may have either + or – symmetry and \tilde{E}_{vL} is the average energy of the v^{th} doublet forming the L -enantiomer. In case of very high potential barriers between the wells corresponding to the two enantiomers, the energetical lower doublets are formed by almost energetically degenerate eigenstates. Then, the approximated energy of these doublets, \tilde{E}_{vL} , becomes exact. Moreover, for a π

¹⁹which is the average energy of the eigenstates $|\Psi_{v+}\rangle$ and $|\Psi_{v-}\rangle$

pulse the amplitudes of the laser field must be chosen such that the complete pulse area A becomes π :

$$A = \int_0^{t_p} \Omega(t) dt = \pi \quad (4.62)$$

Based on expression (4.59) in both simultaneous transitions from the initial pure state $|\Phi_{w\pm}\rangle$ 50% of its population is transferred to $|\Phi_{v+}\rangle$ and 50% to $|\Phi_{v-}\rangle$. Hence, the individual Rabi frequencies Ω_+ and Ω_- for each component of the laser field have to be equal:

$$\Omega_+(t) = \Omega_-(t) \quad \text{with} \quad (4.63)$$

$$\Omega_+(t) = \frac{1}{\hbar\sqrt{2}} \cdot E_+^0 \cdot s(t) \cdot \langle \Phi_{w\pm} | \mu_+ | \Phi_{v\pm} \rangle, \quad (4.64)$$

$$\Omega_-(t) = \frac{1}{\hbar\sqrt{2}} \cdot E_-^0 \cdot s(t) \cdot \langle \Phi_{w\pm} | \mu_- | \Phi_{v\mp} \rangle \quad \text{and} \quad (4.65)$$

$$\Omega(t) = \Omega_+(t) + \Omega_-(t) \neq 0 \quad (4.66)$$

for preparing the target state $|\Psi_{vL}\rangle$. Since the individual pulse areas A_+ and A_- of Ω_+ and Ω_- , as defined in eqn. (4.62), have to be each $\pi/2$ for an overall π transition, the following expressions are obtained for the amplitudes of the laser field components E_+^0 and E_-^0 :

$$E_+^0 = \frac{2\pi\hbar}{\sqrt{2} \langle \Phi_{w\pm} | \mu_+ | \Phi_{v\pm} \rangle t_p} \quad (4.67)$$

$$E_-^0 = \frac{2\pi\hbar}{\sqrt{2} \langle \Phi_{w\pm} | \mu_- | \Phi_{v\mp} \rangle t_p} \quad (4.68)$$

for preparing the target state $|\Psi_{vL}\rangle$. The $|\Psi_{vR}\rangle$ state is not reached, since E_+^0 and E_-^0 are chosen such that eqn. (4.63) and hence, also condition (4.56) holds. For the $|\Psi_{vR}\rangle$ to be prepared, the following expression must be true:

$$\Omega(t) = \pm\Omega_+(t) \mp \Omega_-(t) \neq 0, \quad \text{with} \quad (4.69)$$

$$\Omega_+(t) = -\Omega_-(t) \quad (4.70)$$

and therefore,

$$E_+^0 = \pm \frac{2\pi\hbar}{\sqrt{2} \langle \Phi_{w\pm} | \mu_+ | \Phi_{v\pm} \rangle t_p} \quad (4.71)$$

$$E_-^0 = \mp \frac{2\pi\hbar}{\sqrt{2} \langle \Phi_{w\pm} | \mu_- | \Phi_{v\mp} \rangle t_p}. \quad (4.72)$$

An enantio-selective laser pulse with the parameters (4.67) and (4.68) or (4.71) and (4.72) for the selective preparation of a localized state $|\Psi_{vL/R}\rangle$ corresponding to a pure enantiomer starting from a pure state $|\Phi_{w\pm}\rangle$ can also be used *vice versa*, as anticipated above,

i.e. to select only the desired localized state from an incoherent superposition of $|\Psi_{vL}\rangle$ and $|\Psi_{vR}\rangle$ and transfer its population entirely to any pure state $|\Phi_{w\pm}\rangle$.

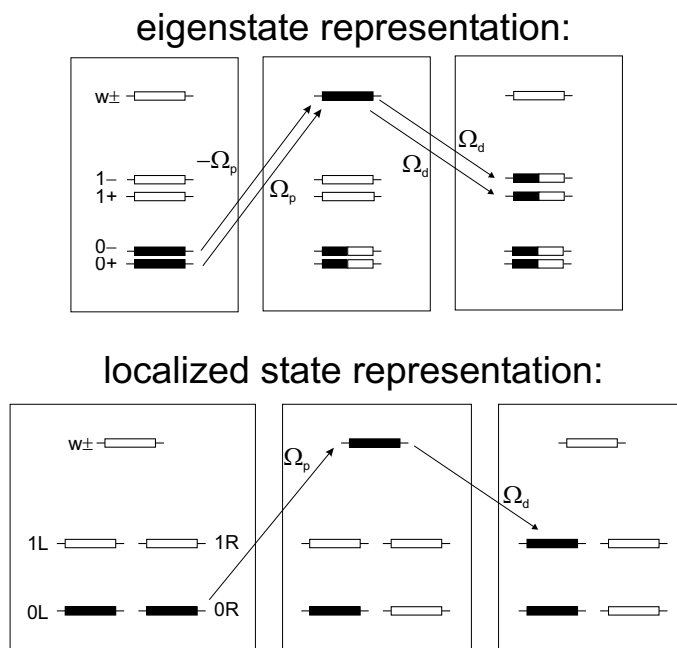


Figure 4.23: Transitions between torsional eigenstates $|\Phi_{v\pm}\rangle$ (top panel) and localized states $|\Psi_{vL/R}\rangle$ (bottom panel) of H₂POSH as induced by a linearly polarized laser pulse sequence consisting of an *R*-selective pump pulse (with Rabi frequency Ω_p) and of a subsequential *L*-selective dump pulse (Ω_d) for the preparation of the pure *L*-enantiomer from a racemate.

Thus, a combination of an enantio-selective pump and an enantio-selective dump pulse can be used to purify a racemic mixture by converting e.g. $|\Psi_{0R}\rangle$ to $|\Psi_{1L}\rangle$ via a pure state $|\Phi_{w\pm}\rangle$ used as intermediate state [137]. Figure 4.23 illustrates the induced transitions of the enantio-selective pump-dump scheme in the torsional eigenstate representation and in the localized state representation for the preparation of a pure *L*-enantiomer.

The choice of the pure state $|\Phi_{w\pm}\rangle$ as intermediate state is crucial for the success of the laser control. In the following section two applications of the enantio-selective pump-dump mechanism are presented, using a torsional eigenstate in the electronic ground or excited state as intermediate state, respectively.

4.7.2 Application of the enantio-selective pump-dump mechanism using IR or UV pulses

The results of the quantum dynamical simulations of the laser induced transformation of the pre-oriented, non-rotating racemate of H₂POSH into pure enantiomers based on the enantio-selective pump-dump mechanism are shown in figures 4.24 and 4.25. The laser pulse parameters and relevant (transition) dipole matrix elements are listed in Table 4.6. Specifically, figures 4.24 and 4.25 show the results using IR or UV pulses which induce transitions between torsional states in the electronic ground state, or between the electronic ground and excited states, respectively. In case of the IR pulses $E_+^0 = E_x^0$ and $E_-^0 = E_y^0$ since $\mu_+ = \mu_x^{00}$ and $\mu_- = \mu_y^{00}$. For the UV transitions $E_+ = E_y^0$ and $E_- = E_z^0$ because $\mu_+ = \mu_y^{01}$ and $\mu_- = \mu_z^{01}$.

In table 4.6 the total field strength of the pulse i is defined as:

$$\overline{E}_i^0 = \sqrt{(E_+^0)^2 + (E_-^0)^2}, \quad (4.73)$$

and the polarization angle α of the linearly polarized pulses is given by:

$$\tan \alpha_i = \frac{E_-^0}{E_+^0}. \quad (4.74)$$

Close inspection of Figures 4.24 and 4.25 shows that the populations of the five states shown in the middle and bottom panels add up to 1 almost perfectly, i.e. all other states are nearly irrelevant. This confirms the efficiency of the enantio-selective pump-dump mechanism explained in the previous section, except for marginal deviations caused by competing excitations of slightly interfering states.

Both IR (Figure 4.24) and UV (Figure 4.25) laser pulses induce the same overall pump-dump mechanism: The first pulse transfers exclusively the undesired enantiomer (here: R, i.e. $|\Psi_{0R}\rangle$) into an excited intermediate state. The subsequent second pulse dumps the population of the intermediate state into local state $|\Psi_{1L}\rangle$ of the target enantiomer, without any significant effect on $|\Psi_{0L}\rangle$. Irrespective of this overall similarity, there are also several significant differences between the IR and UV pump-dump mechanisms, which should have important consequences for the experimental implementations. These concern the laser frequencies, the choice of the intermediate states, the laser pulse durations, the field strength, and the polarizations.

First, the laser frequencies are obviously different for the IR versus UV pump-dump mechanisms. Experimentally available laser pulse frequencies go down to about 500 cm⁻¹

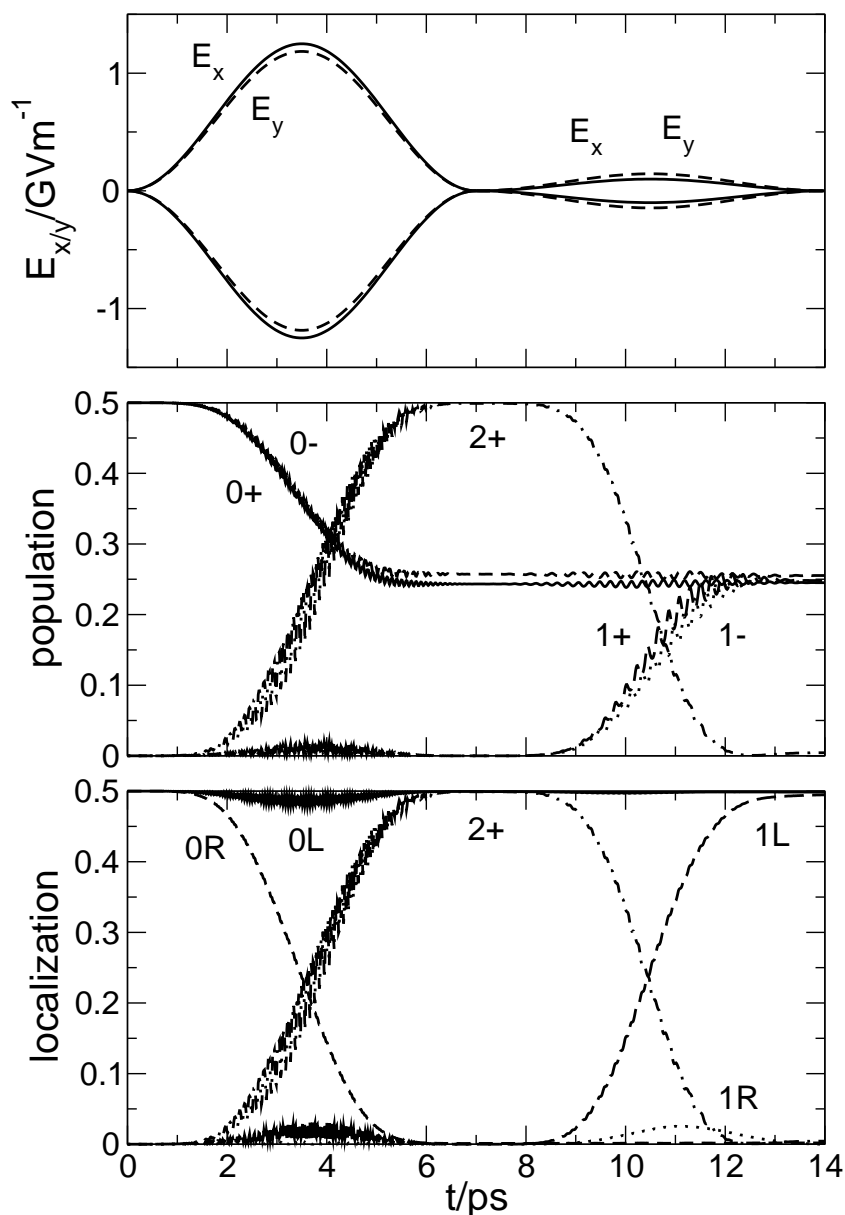


Figure 4.24: Transformation of the model H₂POSH racemate into pure *L*-enantiomers by means of IR enantio-selective pump-dump laser pulses. Top panel: Envelopes of the laser pulses ($E_x = E_+$ and $E_y = E_-$). Middle panel: Populations of the five most important torsional states $|\Phi_{0+}^0\rangle$, $|\Phi_{0-}^0\rangle$, $|\Phi_{1+}^0\rangle$, $|\Phi_{1-}^0\rangle$ and the delocalized intermediate state $|\Phi_{2+}^0\rangle$ (labeled 0+, 0-, ...). Bottom panel: Populations of the local states $|\Psi_{0L}\rangle$, $|\Psi_{0R}\rangle$, $|\Psi_{1L}\rangle$, $|\Psi_{1R}\rangle$ (labeled 0L, 0R, ...) and of the intermediate state $|\Phi_{2+}^0\rangle$. (adapted from ref. [139])

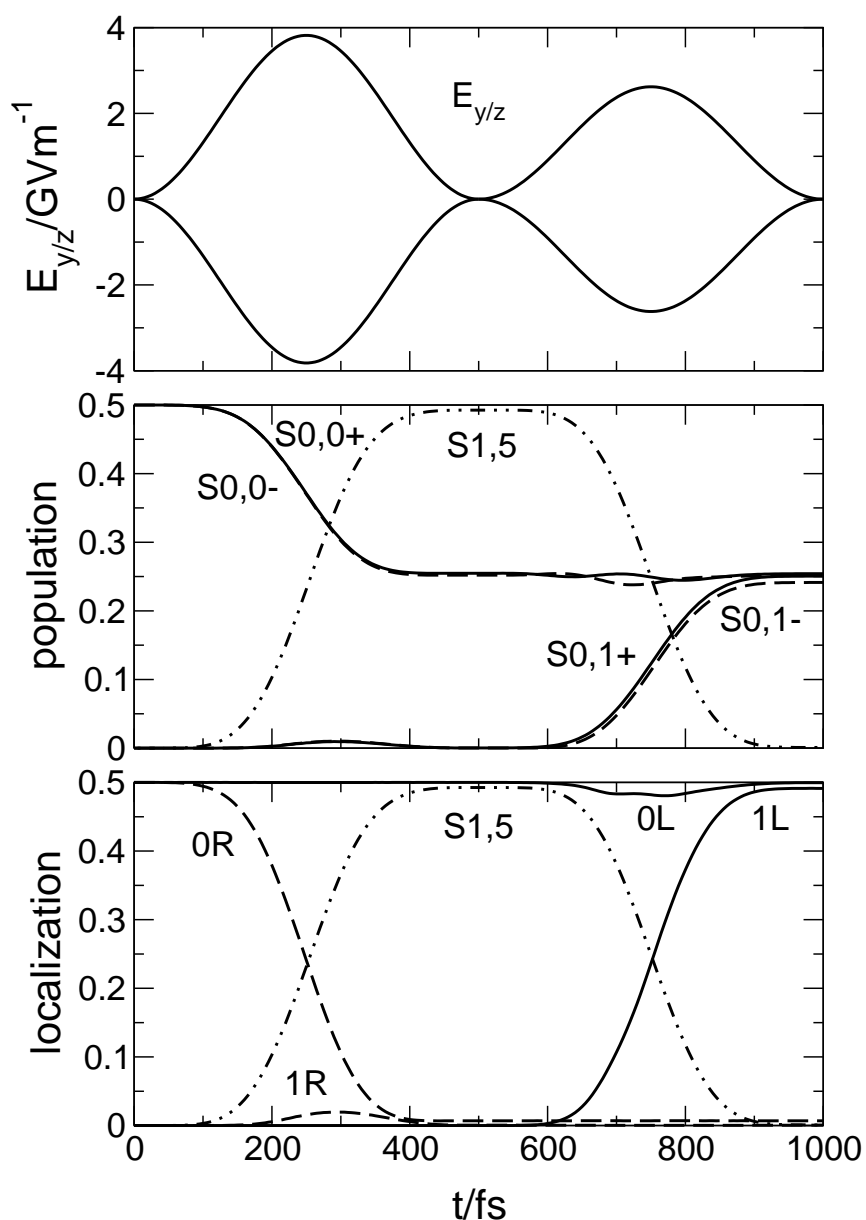


Figure 4.25: Transformation of the model H_2POSH racemate into pure L -enantiomers by means of UV enantio-selective pump-dump laser pulses. Top panel: Envelopes of the laser pulses ($E_y = E_+$ and $E_z = E_-$). Middle panel: Populations of the five most important torsional states $|\Phi_{0+}^0\rangle$, $|\Phi_{0-}^0\rangle$, $|\Phi_{1+}^0\rangle$, $|\Phi_{1-}^0\rangle$ and the excited intermediate state $|\Phi_5^1\rangle$ (labeled $S0,0+$; $S0,0-$; ...). Bottom panel: Populations of the local states $|\Psi_{0L}\rangle$, $|\Psi_{0R}\rangle$, $|\Psi_{1L}\rangle$, $|\Psi_{1R}\rangle$ (labeled $0L, 0R, \dots$) and of the intermediate state $|\Phi_5^1\rangle$. (adapted from ref. [139])

Table 4.6: Dominant transitions, (transition) dipole matrix elements, and pump-dump laser pulses for the transformation of the H₂POSH model racemate into pure enantiomers. (adapted from ref. [139])

property/parameter	IR pump	IR dump	UV pump	UV dump
dominant transition	$ \Phi_{0+}^0\rangle \rightarrow \Phi_{2+}^0\rangle$	$ \Phi_{2+}^0\rangle \rightarrow \Phi_{1+}^0\rangle$	$ \Phi_{0+}^0\rangle \rightarrow \Phi_{5(-)}^1\rangle$	$ \Phi_5^1\rangle \rightarrow \Phi_{1+}^0\rangle$
(transition) dipole matrix element/ ea_0	$\langle \Phi_{0+}^0 \mu_{+}^{00} \Phi_{2+}^0 \rangle$ $-6.7582 \cdot 10^{-3}$	$\langle \Phi_{2+}^0 \mu_{+}^{00} \Phi_{1+}^0 \rangle$ $-89.581 \cdot 10^{-3}$	$\langle \Phi_{0+}^0 \mu_{-}^{01} \Phi_5^1 \rangle$ $+29.929 \cdot 10^{-3}$	$\langle \Phi_5^1 \mu_{-}^{01} \Phi_{1+}^0 \rangle$ $-42.244 \cdot 10^{-3}$
coupled to laser field	$E_{+}^0(\text{IR},x)$	$E_{+}^0(\text{IR},x)$	$E_{-}^0(\text{UV},z)$	$E_{-}^0(\text{UV},z)$
field amplitude E_i^0/GVm^{-1}	1.25	0.10	3.82	-2.62
frequency $\omega_i/2\pi c \cdot cm^{-1}$	343.90	156.51	44252.35	44066.66
phase $\eta_i/^\circ$	0	0	0	0
dominant transition	$ \Phi_{0-}^0\rangle \rightarrow \Phi_{2+}^0\rangle$	$ \Phi_{2+}^0\rangle \rightarrow \Phi_{1-}^0\rangle$	$ \Phi_{0-}^0\rangle \rightarrow \Phi_5^1\rangle$	$ \Phi_5^1\rangle \rightarrow \Phi_{1-}^0\rangle$
(transition) dipole matrix element/ ea_0	$\langle \Phi_{0-}^0 \mu_{-}^{00} \Phi_{2+}^0 \rangle$ $+7.1303 \cdot 10^{-3}$	$\langle \Phi_{2+}^0 \mu_{-}^{00} \Phi_{1-}^0 \rangle$ $-55.517 \cdot 10^{-3}$	$\langle \Phi_{0-}^0 \mu_{+}^{01} \Phi_5^1 \rangle$ $-29.945 \cdot 10^{-3}$	$\langle \Phi_5^1 \mu_{+}^{01} \Phi_{1-}^0 \rangle$ $+43.854 \cdot 10^{-3}$
coupled to laser field	$E_{-}^0(\text{IR},y)$	$E_{-}^0(\text{IR},y)$	$E_{+}^0(\text{UV},y)$	$E_{+}^0(\text{UV},y)$
field amplitude E_i^0/GVm^{-1}	1.185	0.145	3.82	2.62
frequency $\omega_i/2\pi c \cdot cm^{-1}$	343.90	156.51	44252.35	44066.66
phase $\eta_i/^\circ$	0	41	0	0
duration t_{p_i}/ps	7.0	7.0	0.5	0.5
total field amplitude \bar{E}_i^0/GVm^{-1}	1.7224	0.1761	5.4023	3.7052
intensity ^a $I_i/TWcm^{-2}$	0.78748	0.0082317	7.7469	3.6441
polarization angle $\alpha_i/^\circ$	+43.47	+55.41	+45	-45

^aThe intensity is proportional the square of the amplitude $I = \varepsilon_0 \cdot c \cdot |\bar{E}^0|^2$. In general, intensities higher than $10 TWcm^{-2}$ may cause dissociation or ionisation of the molecules [134].

[140].²⁰ Hence, the IR laser pulses presented here cannot be realized experimentally nowadays. Second, the choice of the intermediate excited states $|\Phi_{w\pm}\rangle$ for IR transitions in the electronic ground state e.g. $|\Phi_{0+}^0\rangle \rightarrow |\Phi_{w\pm}^0\rangle \rightarrow |\Phi_{1+}^0\rangle$, or $|\Phi_{w(\pm)}^1\rangle$ for UV transitions via electronic excited state e.g. $|\Phi_{0+}^0\rangle \rightarrow |\Phi_{w(\pm)}^1\rangle \rightarrow |\Phi_{1+}^0\rangle$ is based on conditions (4.67-4.72) for π pulses. Accordingly, the most efficient sequential IR or UV pulses should be associated with the largest products of (transition) dipole matrix elements, $\langle\Phi_{0+}^0|\mu_+^{00}|\Phi_{w+}^0\rangle \times \langle\Phi_{w+}^0|\mu_+^{00}|\Phi_{1+}^0\rangle$ or $\langle\Phi_{0+}^0|\mu_-^{01}|\Phi_{w-}^1\rangle \times \langle\Phi_{w-}^1|\mu_-^{01}|\Phi_{1+}^0\rangle$, respectively. This criterion yields $|\Phi_{2+}^0\rangle$ as intermediate state for IR transitions i.e. the pump pulse excites the first torsional overtone, followed by the dump transition to the fundamental excited torsional state. The corresponding matrix elements differ by approximately one order of magnitude (see Table 4.6), calling for much stronger field strengths of the pump pulses than for the dump pulses, see Figure 4.24 and Table 4.6. Alternatively, one may also use $|\Phi_{2-}^0\rangle$ as intermediate state, whereas higher excited states are not recommended because they would require even higher overtone excitations with higher intensities due to smaller transition dipole matrix elements. The same criterion yields $|\Phi_{5(-)}^1\rangle$ as intermediate state for the UV transition. This may be interpreted as a consequence of preferably near-vertical Franck-Condon type transitions between the initial, intermediate, and final states. An important difference between the IR and UV transitions is, therefore, that the intermediate state in UV transitions carries more torsional quanta (five) than for the IR transition (two). As a consequence, the density of states close to the intermediate state is much higher for UV than for IR transitions. Therefore, the selectivity of the IR laser pulses should be better than for the UV transitions, which could excite also near resonant, non-torsional states. However, the electronic excited state S_1 has recently been found to be repulsive along the P-S coordinate with a dissociation time of the order of 100 fs [130]. Hence, most of the population of the intermediate state $|\Phi_5^1\rangle$ in S_1 will be destroyed by dissociation within the time of the dump pulse. This decreases the efficiency of the pump-dump mechanism via an intermediate state in the S_1 but also opens up the opportunity for intentional destroying of the undesired enantiomer (for further discussion see the next section).

Third, the required laser pulse durations and field strength turn out to be longer and higher for IR laser pulses than for UV pulses. This is again a consequence of the corresponding products of (transition) dipole matrix elements which are smaller for IR than for UV pulses. For the selected excited intermediate states one gets e.g. (see Table 4.6):

$$|\langle\Phi_{0+}^0|\mu_+^0|\Phi_{2+}^0\rangle \times \langle\Phi_{2+}^0|\mu_+^0|\Phi_{1+}^0\rangle| < |\langle\Phi_{0+}^0|\mu_-^1|\Phi_5^1\rangle \times \langle\Phi_5^1|\mu_-^1|\Phi_{1+}^0\rangle| \quad (4.75)$$

²⁰Laser pulses with frequencies below 500 cm^{-1} can be generated in thin GaSe crystals by optical rectification of ultrashort laser pulses [141]. However, the energies of these far-infrared pulses are only of the order of pJ.

The conditions (4.67–4.72) for π -pulses then imply that the corresponding products of laser field durations times field strengths should be larger for IR than for UV pulses. For example, the applications shown in figures 4.24 and 4.25 use 7 ps versus 0.5 ps pulse durations for IR versus UV pump pulses, respectively, with similar field strengths.

Forth, the polarizations of the IR versus UV pump and dump pulses are also different. In most cases, linearly polarized pulses achieve high enantiomer selectivities, but for the IR dump pulse a phase shift of 41° (see Table 4.6) implying an elliptical polarization is found to be more efficient. For the present linearly polarized pulses ($\eta = 0$ in Table 4.6), the polarization angles α_i are determined by eqn. (4.74) as arctan of the ratios of the + and – (transition) dipole matrix elements which are associated with the transitions between two doublet states $|\Phi_{0+}^0\rangle$ or $|\Phi_{0-}^0\rangle$ (and likewise $|\Phi_{1+}^0\rangle$ and $|\Phi_{1-}^0\rangle$) and the excited intermediate state. From Table 4.6, the resulting polarization angles are close to -45° and $+45^\circ$ for the UV pump and dump pulses, i.e. the UV pump and dump laser pulses have near orthogonal polarizations, see also the discussion in ref. [137]. A systematic investigation of UV transitions via other, less efficient intermediate states reveals, however, that this near orthogonal polarization is not a general rule. Instead it may be interpreted as a consequence of the incidental near coincidence of the transition dipole functions μ_y^{01} and μ_z^{01} close to the near vertical UV-transitions involved, see figure 4.7. In contrast, the polarization angles for the most efficient IR pump and dump pulses are $+43.47^\circ$ and $+55.41^\circ$ (see Table 4.6), i.e. they are non-orthogonal.

The enantio-selective pump-dump mechanism has in the previous simulations proven to be a very effective way for the purification of a racemate of oriented molecules. In comparison with the parking mechanism it has several advantages. First, no “parking” state is needed where the “parked” population has to “wait” unaffected until it is deexcited. In a real system this is a restriction to the feasibility of the laser control since the choice of this “parking” state is crucial for the success of the experiment. Second, the overall duration of the complete pulse sequence is much shorter in case of the enantio-selective pump-dump scheme preventing IVR. Third, the number of subpulses to control the molecule is decreased drastically, from five subpulses in the parking scheme to two in the enantio-selective pump-dump, and therefore, the effectiveness of the laser control is increased. In summary, the enantio-selective pump-dump mechanism is an excellent approach towards an experimental realization of laser pulse controlled racemate purification.

In the following section an experimental proof for the simulated purification of a racemic mixture of pre-oriented H₂POSH molecules by ultra-short laser pulses based on the enantio-selective pump-dump mechanism will be suggested.

4.8 A proposed experimental proof

So far different laser control mechanism to convert a racemate into a pure enantiomer have been suggested. All simulations have proven that these control schemes can successfully be applied to the model system H₂POSH. The real proof would be, of course, a successful experiment in a laboratory. Among the difficulties to realize the purification of a racemate by laser control is the probing of the prepared pure enantiomer: the density of molecules in the gas phase, e.g. a molecular beam, is very low for using circular dichroism spectroscopy and standard pump-probe as well as IR/UV spectroscopy cannot discriminate between two enantiomers. Hence, an experimental setup showing that the racemate is purified is needed. In figure 4.26 a series of experiments is sketched for this purpose.²¹

Each experiment starts from pre-oriented H₂POSH molecules at low temperature under the influence of a single enantio-selective pump pulse, i.e. the first step of the previously discussed enantio-selective pump-dump scheme. This single laser selectively excites one mirror form of the molecules (leaving the other one untouched) so that the chiral pair is no longer energetically degenerate. Based on energetic criteria, a sequential reaction can then distinguish the *L*- from the *R*-enantiomer, for instance dissociating one enantiomer. In this situation it is possible to discriminate the excited enantiomer from the untouched enantiomer by employing mass spectroscopy. In case of a racemic mixture, see first case in figure 4.26, peaks of fragments and the molecular peak of the untouched molecules will appear in the mass spectrum after photo-ionization. No information about which chiral form has been dissociated can be obtained from this single experiment. Therefore, two more experiments have to be carried out starting from the pure *L*- and *R*-enantiomer, each time employing the same enantio-selective (here *L*-selective) pump-pulse followed by dissociation. In case of pure *R*-enantiomers the enantio-selective pulse has no effect on the molecules and hence, no dissociation should take place. The mass spectrum should thus show no fragments of dissociated molecules but a higher molecular peak in comparison with the first experiment. In case of only pure *L*-enantiomers the opposite effect should be observed. Since the enantio-selective pump pulse now excites all molecules, all of them should be dissociated in the subsequent reaction, showing peaks for the produced fragments but no molecular peak in the mass spectrum. The combination of these three experiments allows the laboratory identification of the prepared enantiomer and hence, proofs that the enantio-selective laser pulse was successful.

²¹Fruitful discussions with J. Thieke are acknowledged.

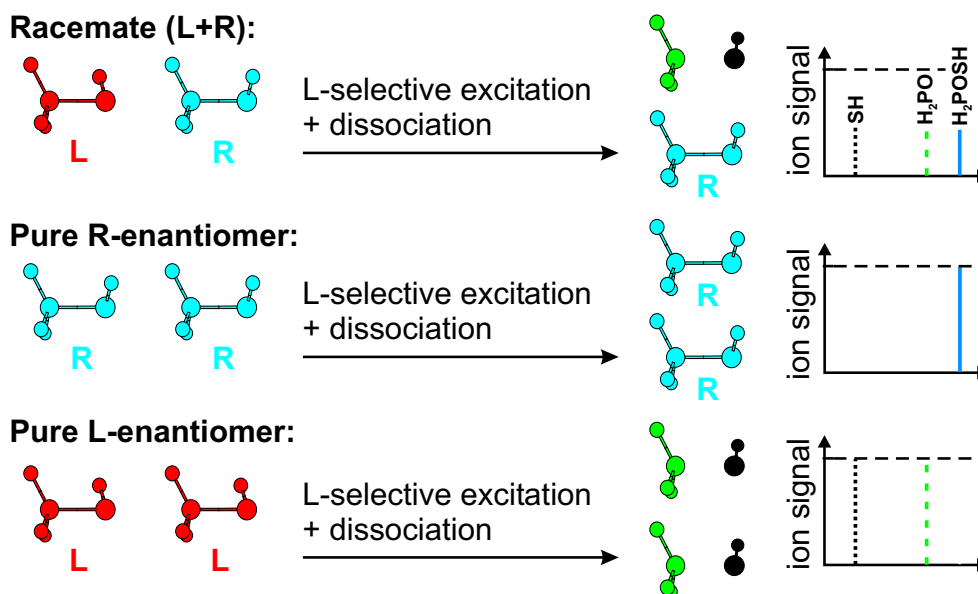


Figure 4.26: A proposed experimental proof for the success of enantio-selective laser pulses. An enantio-selective excitation eliminates the energetic degeneracy of the two enantiomers. The products of a subsequent photo-destruction of the energetically excited undesired form can be detected by e.g. mass spectroscopy. The detected products of the shown three experiments proof indirectly the success of the enantio-selective laser pulse (adapted from ref. [130]).

Of course, the experiments proposed in fig. 4.26 characterize a perfect scenario which can never be accomplished in a laboratory. In order to perform mass spectroscopy the molecules are usually ionized initiating subsequent fragmentation of the ionized species. Thus, in each experiment peaks of all kinds of fragments will appear in the mass spectrum. Nevertheless, if these experiments are carried out carefully, the comparison of the three mass spectra should give the desired information. If the enantio-selective laser control is unsuccessful all three mass spectra should be almost identical.

Still, more obstacles have to be surpassed before the proposed experiment can be carried out. For the chosen model system H₂POSH the electronic excited state S_1 has indeed been found to be dissociative by recent *ab initio* calculations carried out by Shibl and González [130]. Therefore, a single enantio-selective pump pulse could excite the desired enantiomer from a racemate to the excited state where it will dissociate within a certain time.²² This enantio-selective excitation can also be done in a two step mechanism dis-

²²Further investigations using a 2D model system are currently performed by M. F. Shibl, L. González

cussed in the next chapter (see ref. [130]). However, the proposed experiments require that the initial species do not racemize quickly, i.e. stable enantiomers could be prepared by chemical means before the laser control experiment. Here, the chosen model system H₂POSH is not an ideal candidate since its torsional barrier is so low that no pure enantiomer can be isolated at room temperature. Even at very low temperature it is doubtful that a pure enantiomer could be prepared in a laboratory by chemical means. Hence, a molecule which forms stable enantiomers and which can be synthesized by an enantioselective chemical reaction or purified by chemical means is required.²³ In the following chapter, a new model system is introduced which is more appropriate for a plausible experiment. The enantio-selective excitation briefly introduced in this section will be discussed in more detail deriving a modification of the enantio-selective laser control.

and J. Manz.

²³Hence, a molecule that also satisfying criteria (d) and (f) for the choice of a “good” model system (see section 4.2) is desired.